THE CONCEPT OF VIRTUAL EVENTS:
APPLICATION TO THE ATTENUATION OF INTERNAL MULTIPLES

A Thesis

by

ILANA EREZ

Submitted to the Office of Graduate Studies of
Texas A&M University
in partial fulfillment of the requirements for the degree of

MASTER OF SCIENCE

August 2006

Major Subject: Geophysics

THE CONCEPT OF VIRTUAL EVENTS:

APPLICATION TO THE ATTENUATION OF INTERNAL MULTIPLES

A Thesis

by

ILANA EREZ

Submitted to the Office of Graduate Studies of
Texas A&M University
in partial fulfillment of the requirements for the degree of

MASTER OF SCIENCE

Approved by:

Chair of Committee,	Luc T. Ikelle
Committee Members,	Thomas A. Blasingame
	Mark E. Everett
Head of Department,	Richard L. Carlson

August 2006

Major Subject: Geophysics

ABSTRACT

The Concept of Virtual Events:
Application to the Attenuation of Internal Multiples. (August 2006)
Ilana Erez, B.Sc., Tel Aviv University, Israel
Chair of Advisory Committee: Dr. Luc T. Ikelle

Modern seismic imaging tools for oil and gas exploration and production (E&P) assume that seismic data contain responses only of waves that bounce (e.g., reflect, diffract) only once at each interface in the subsurface. This type of response is called a primary. Unfortunately, actual seismic data also contain responses of waves that bounce at several interfaces in the subsurface. This type of response is called a multiple.

In general, multiples in seismic data fall into two categories: (1) events that bounce at least once at the free surface in addition to any other bounce in the subsurface and (2) events that do not bounce at the free surface but instead inside the subsurface, at two or more interfaces. The first category has the greater amount of energy; therefore most of the research and development efforts in E&P have so far focused on attenuating this category of multiples accurately.

At present, more knowledge of the subsurface is expected from seismic imaging. To avoid any misinterpretation of these details, there is a growing need in the E&P industry to also attenuate the second category of multiples, known as internal multiples.

In this work I describe a new method of attenuation of internal multiples. The method consists of predicting the internal multiples and then subtracting them from the data. The prediction of internal multiples from seismic data is made possible by the discovery of a new type of seismic scattering event known as a virtual event.

Seismic virtual events constitute a calculational device, which is becoming an important part of seismic data processing. Virtual events combine forward and backward wave propagation in such a way that their convolution with real events allows us to predict internal multiples.

In addition to showing how virtual events can be constructed from real seismic events, I also show that virtual events obey physical laws, despite their counterintuitive wavepath.

I have illustrated the findings in this thesis with synthetic examples. In particular, I have shown the effectiveness of my internal-multiple-attenuation method for a 1D data set, which includes several primaries and internal multiple interferences.

To my parents, Michael and Lyubov, and my brother, Alex.

ACKNOWLEDGMENTS

It is a pleasure to thank my academic advisor and chair, Dr. Luc T. Ikelle for his financial and moral support. His guidance and active assistance was indispensable to the completion of this program. I appreciate his willingness to spend his valuable time in guiding me through my thesis.

I would also like to express my gratitude to my committee members: Dr. Blasingame and Dr. Everett, who included me in their busy schedules. I sincerely thank Dr. Gangi for his comments and for agreeing to substitute for Dr. Everett during my thesis defense.

Acknowledgments are also due to all the sponsors of the CASP project for providing the fundings for this research. My appreciation also goes to all the CASP members for their help, and in particular to Shantanu Kumar Singh. My special thanks to the computer systems manager, Steve Tran, for countless hours of help.

Last, but most importantly, I would like to thank my extended family for their constant support and encouragement, and especially my husband Noam who always believed in me, and my 2-year old son Danny for lighting up our home and for not interfering with my work as much as he could.

TABLE OF CONTENTS

CHAPTER Page

LIST OF FIGURES

FIGURE Page

FIGURE Page

FIGURE Page

CHAPTER I

INTRODUCTION: ORIGIN OF SEISMIC VIRTUAL EVENT

Seismic virtual events constitute a calculational device which is becoming an important part of seismic data processing. These events have already established application to internal-multiple removal. Seismic virtual events have a real physical basis, and their roots are in the representation theorem; they follow physical laws and are created from real seismic events. However, they cannot be recorded directly with current acquisition technology.

Seismic virtual events got their name from quantum physics by analogy with *virtual particles*. Quantum virtual particles cannot be detected by measurement devices but play a fundamental part in quantum field theory, just like seismic virtual events might do one day in seismic processing.

My goal in this chapter is to review the origin of a virtual event – its motivation and its construct. I will start the first section by providing a brief review of real seismic events. In the second section, I show the motivation for construction of virtual events. In the third section, I introduce virtual events and its scattering diagrams. In the last section, I present potential applications of virtual events in seismic processing.

1. Brief background on real seismic events

For clarity and consistency, allow me to introduce a brief summary of real seismic events before discussing virtual events.

A direct wave is an event that goes from the source directly to the receiver without hitting either the subsurface or the free surface [Figure 1 (a)]. This event is

---

This thesis follows the style of Geophysics.

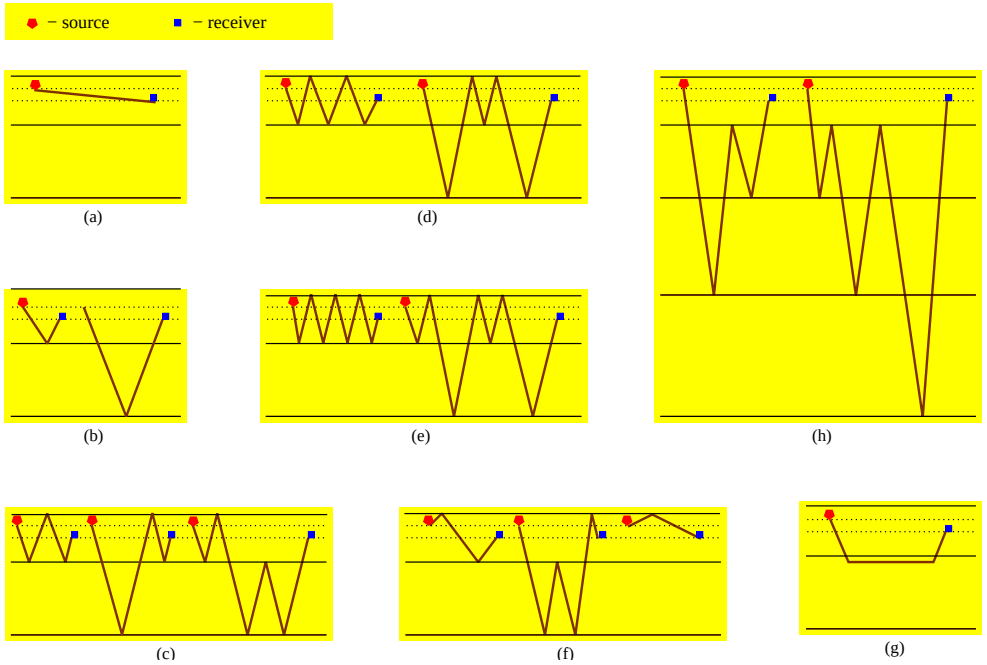

Figure 1. Examples of seismic events: (a) is a direct wave, (b) are primaries, (c), (d), and (e) are first-, second- and third-order free-surfaces multiples, respectively, (f) are ghosts, (h) are internal multiples, and (g) is a refraction.

usually easy to remove from the data when needed.

A primary is an event that goes from the source to the scattering point and then from the scattering point to the receiver [Figure 1 (b)]. Note that this event contains only one scattering point in the subsurface and does not bounce at the free surface. Primaries bring convenient and sufficient information about the subsurface structure. Unfortunately, seismic acquisitions cannot avoid recording events other than primaries. Seismic processing usually focuses on attenuating other events and emphasizing primaries.

Free-surface reflections are divided into free-surface multiples and ghosts. They are unwanted events, and different methods of attenuating them are suggested by scientists all over the world. In the next chapter of my thesis I am going to discuss one such method and use it for further research.

A ghost is an event that has a bounce at the free surface as its first or/and last reflection [Figure 1 (c)].

A free-surface multiple is an event that bounces twice or more at scattering points in the subsurface and bounces at least one time (but not the first bounce or the last bounce) at the free surface.

First-order free-surface multiples bounce at the free surface one time [Figure 1 (d)].

Second-order free-surface multiples bounce at the free surface two times [Figure 1 (e)].

Third-order free-surface multiples bounce at the free surface three times [Figure 1 (f)], and so on.

An internal multiple is an event that reflects from a few scattering points without

bouncing at the free surface [Figure 1 (g)]. Although this event does not have strong amplitude, it still needs attenuating. But such a technique is hard to develop because all the scattering points are located at the subsurface, in contrast to free-surface multiples and ghosts, which include at least one scattering point at the free surface. In the next chapter, I will review a technique to attenuate internal multiples using virtual events.

A refraction is an event that goes from the source at a critical angle, travels along an interface between layers in the subsurface, and then goes to the receiver [Figure 1 (h)]. Events that contain a refraction and at least one bounce at the free surface are included in free-surface reflections. All other refractions can be considered internal multiples because they have more than one scattering point in the subsurface and no bounce at the free surface.

2. Motivation for construction of seismic virtual events

The process of removing internal multiples is similar to the one for removing free-surface multiples in the sense that both processes are based on the idea of constructing multiples and then subtracting them from the data. When constructing free-surface multiples, wave-propagation paths of different events of the data are combined, because wave-propagation paths of free-surface multiples contain at least one reflection point at the free surface. Unfortunately, such a construction is not possible for internal multiples, as we will see in the next paragraph.

According to Ikelle (2006), there are three major differences between internal and free-surface multiples that make internal multiple attenuation very tricky:

1. The interface generating free-surface multiples is known – it is the free surface.

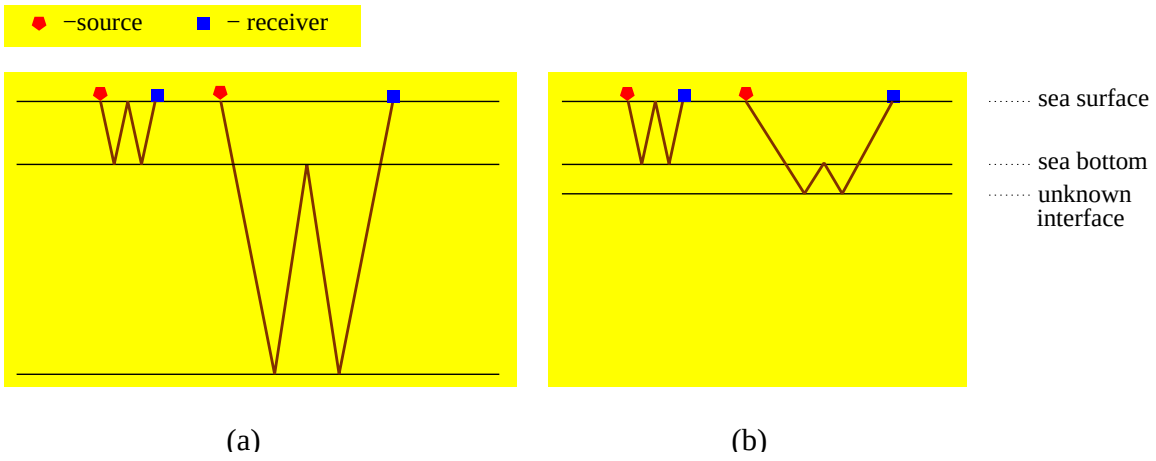

Figure 2. An illustration of the predictable period of free-surface multiples, and the unpredictably short (a) or long (b) period of internal multiples.

The interface generating internal multiples can be any subsurface interface that we don't know about. And that leads us to the next two differences:

2. If the acquisition is marine, we know the smallest period of free-surface multiples – it is the two-way traveltime in the water column. But since we don't know the subsurface structure (the goal of seismic processing is to find the subsurface structure), the smallest period of an internal multiple can be very long [Figure 2 (a)] or very small, almost the length of a primary [Figure 2 (b)].

3. To construct free-surface multiples, the wave propagation has to be extrapolated from the sensor locations to the surface, using the velocity of the water, as the sensors are located in the water layer. But this cannot be done for internal multiples, since wavefield extrapolation from a scattering point to the sensor locations requires knowledge of the velocity model between the scattering point and the sensor locations.

Working under the assumption that the subsurface is unknown is difficult and

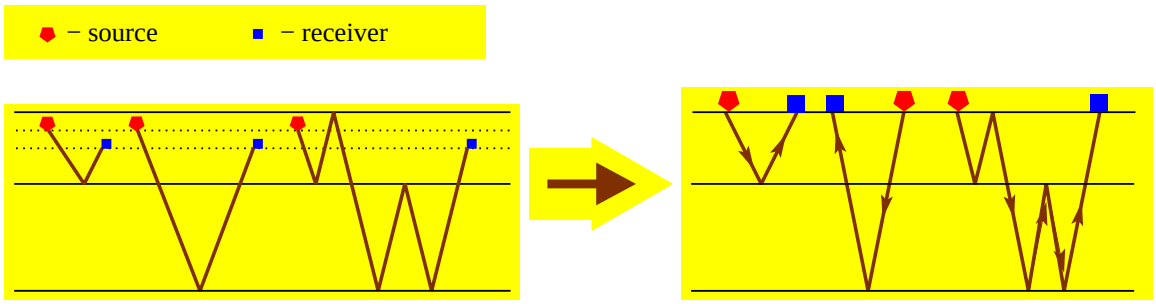

Figure 3. The conventions for this thesis: source and receiver are located on the surface, and the arrows define the direction of the raypath.

unpleasant. That is the reason for Ikelle's suggestion that the way to treat the problem is to bring the data about internal multiples to the surface (Ikelle, 2006). Because that is actually what the virtual event does: it brings knowledge about the scattering point to the surface.

3. Constructing a virtual event

A. Conventions

I will introduce a few conventions related to scattering diagrams in order to facilitate the reading of these diagrams.

1. In my thesis the scattering diagrams for construction of real and virtual events will appear with sources and receivers located on the surface [Figure 3]. In other words, we assume that the data have been extrapolated to the surface. It does not have to be a free surface, because there is no emphasis on free-surface reflections, in this thesis we just want to make sure that the source and the receivers are on the same level.

2. So far I have displayed scattering diagrams without indicating the direction of

the wave propagation because I have implicitly assumed forward wave propagation only. As we will see in the next section, virtual events involve forward and backward wave propagation. For that reason I include arrows in my scattering diagrams, as depicted in Figure 3. Arrows going from left to right indicate forward propagation, and arrows going from right to left indicate backward propagation.

3. All seismic events (including those on virtual fields, as will be discussed later) must obey Snell's law. Although, for clarity, the scattering diagrams in my thesis do not obey this law in drawing seismic events, all the calculations and discussions in my thesis do so.

B. Crosscorrelating data

Let us assume we have seismic data free of direct waves and free-surface reflections. The data consist of pressure field $P(x_r, x_s, \omega)$ recorded by hydrophone, and the vertical component of particle velocity $V(x_r, x_s, \omega)$, recorded by geophone for the receiver at x_r, for the source point at x_s and for frequency ω. The field of virtual events is defined as follows (Ikelle, 2006):

$$P_v(x_r, x_s, \omega) = \int_{-\infty}^{+\infty} dx P^*(x_r, x, \omega) V(x, x_s, \omega) \tag{1.1}$$

where $P_v(x_r, x_s, \omega)$ is the field of virtual events and the asterisk $*$ denotes a complex conjugate. Note that instead of multiplication of two data fields (convolution in the time domain, which is common operator in multiple attenuation), we have multiplication of data with complex conjugate, which makes it a crosscorrelation in the time domain. The integral over x makes the crosscorrelation multidimensional. Figure 4 (a) shows an illustration of the formula (1.1) in the time-space domain using the

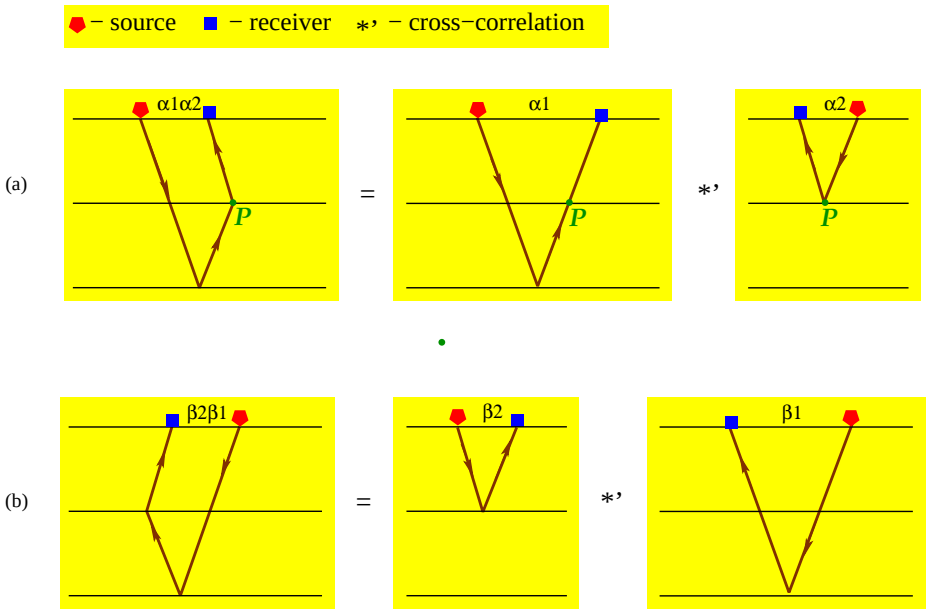

Figure 4. Construction of virtual event by cross-correlation of two primaries: (a) – when α_1 is going forward in time, and α_2 is going backward in time, the event $\gamma_1 = \alpha_1\alpha_2$ is going forward in time; (b) – when β_2 is going forward in time, and β_1 is going backward in time, the event $\gamma_2 = \beta_2\beta_1$ is going backward in time.

scattering diagrams. We basically crosscorrelate two primary events, α_1 and α_2, to produce a virtual event, $\gamma_1 = \alpha_1\alpha_2$. Crosscorrelation is taking the place of convolution to flip the second event in time. While α_1 is going forward in time, event α_2 is time-reversed. The wave-propagation paths of the events meet at the receiver point of primary α_1, and the source point of primary α_2. The part of event α_1 from point P to the receiver cancels out the part of event α_2 from the source to point P, and a virtual event is constructed.

As an analogy, think of a videoplayer playing seismic events. Primary α_1 would appear as a regular forward-playing movie (activated by the play button), whereas primary α_2 would appear as a reverse-playing movie (activated by the reverse button). So the videoplayer is playing event α_1 and then immediately event α_2; and you can see that as event α_2 starts, it is playing the reverse of the event α_1 up to point P, and then it continues playing α_2 as a reversed movie. In terms of time, since we cannot go back in time in real life, the time-reversed event α_2 propagates from the end to beginning (i.e., it starts at the receiver point and goes to the source point) in such a way, that it reaches point P at exactly the same time as does event α_1. So in a causal environment we see that event α_2 starts propagating before event α_1 hits the first interface; then they meet at point P and stop there.

Remember that crosscorrelation is not a commuting operator. Figure 4 (b) demonstrates crosscorrelation of the same events as on Figure 4 (a), but switched between them in such a way that event β_2 is now going backward in time, and event β_1 is going forward in time. The outcome is an anti-causal virtual event, $\gamma_2 = \beta_2\beta_1$, which can be compared to the causal virtual event γ_1 in Figure 4 (a) . In other words, we can create forward-propagating virtual events as well as backward-propagating virtual events.

Let us look at the virtual events for 1D data. The geological model on Figure

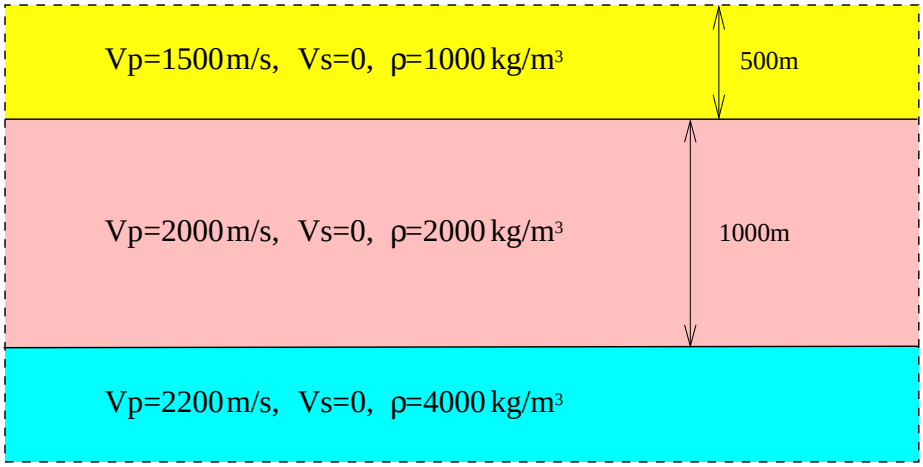

Figure 5. 1D subsurface structure for data simulation

5 is used to simulate the 1D data in Figures 6 and 7. Figure 6 is the pressure data; it contains two primaries, α_1 and α_2, and a refraction, α_3. Figure 7 is the vertical component of partical velocity; it contains the same events as the previous data field named β_1, β_2 and β_3. The crosscorrelation of the pressure data field with velocity data field produces field of virtual events [Figure 8]. There are three events on the virtual field: γ_1 represents the autocorrelation of the first, second and third events; γ_2 represents the crosscorrelation of event α_2 with event β_1; and γ_3 represents the crosscorrelation of event α_3 with event β_1. The autocorrelation γ_1 looks pretty much like a direct wave on a real field, so we call it virtual direct wave. The virtual reflection γ_2 resembles the form of a real reflection. And the refraction-reflection event γ_3 (virtual refraction) is separated from the related reflection event γ_2, unlike real reflections and refractions.

Note that the virtual field has its weakness at the far offset, because crosscorrelation leaves gaps at the far offset, just like the convolution leaves gaps at the near offset. As you can see in Figure 9 (a), convolutions expand data, extending offsets

from 100m to 200m; however, if the minimum data are 100m, they cannot produce smaller offset data. On the other hand, crosscorrelation compresses data, as shown in Figure 9 (b), reducing offsets from 200m to 100m; but if the maximum offset is 200m, the offset of virtual events will always be smaller. Therefore, to build far offsets on virtual field, we need "farther" offsets on real fields.

Let us remark that the seismogram of the virtual events in Figure 8 shows only positive-time part of the field. The negative-time part, which is complex conjugate of the positive-time in the F-X domain, is not shown for one simple reason: the parts are symmetrical. For example, Figure 10 draws scattering diagrams to explain the events in Figure 8. Events γ_1, γ_2, and γ_3 are the events depicted in Figure 8 (c). However, events γ_{22} and γ_{33} in Figure 10 are not shown on the data in Figure 8 (c): γ_{22} is totally symmetrical with γ_2, and so are γ_{33} and γ_3, but according to the arrows, the first one in each couple goes back in time. Thus we do not show negative times in data, keeping in mind that every event in the virtual field has his symmetrical twin brother with respect to time equals 0.

Until recently (for example, in Figure 4), when I used the expression "virtual events", I meant "virtual reflection", as I did in Figure 4. But as you see from the previous example, virtual scattering holds every kind of virtual events: there are virtual reflections (primary and multiples), virtual refractions, even virtual direct wave, and if we do not use the convention of extrapolation of the events to the free surface, there will be virtual ghosts. The emphasis at virtual reflection in the beginning of this chapter serves an historical purpose only: this is how the study of virtual field began.

4. Conclusions

Multidimensional crosscorrelation of different primaries, multiples, refractions, and even direct waves can produce virtual fields with different kinds of weird-looking events [Figure 11]. Although we still do not know how to use most of them, they surely can be potential problem solvers. For example, the event in Figure 11 (e) can be very useful because of the analogy with the equivalent light ray, which is very useful in optics.

Applications in Figures 12 and 13 are for the attenuation of internal multiples, which I will discuss in Chapter III, and the separation of reflected and refracted waves.

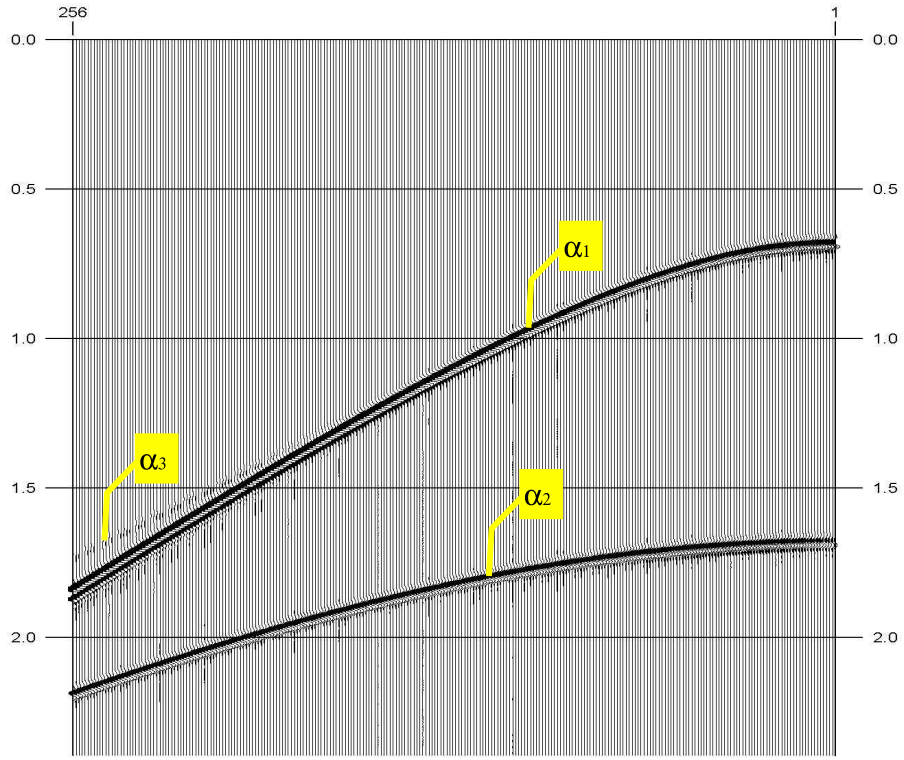

Figure 6. Pressure data field including three events: two primaries and one refraction.

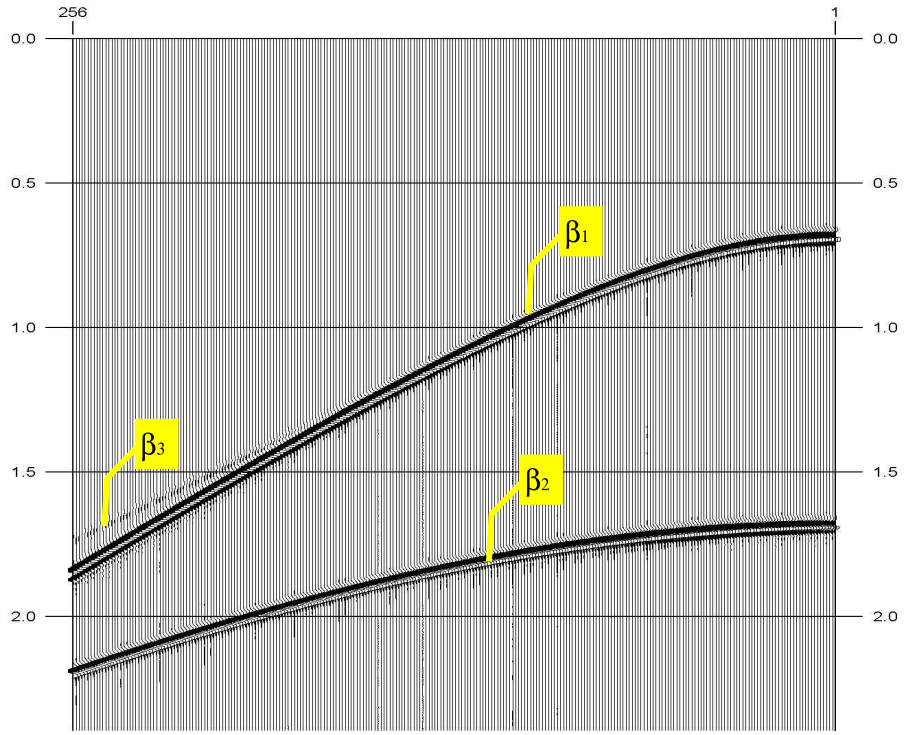

Figure 7. Vertical component of partical velocity data field including the same three events as the pressure data: two primaries and one refraction.

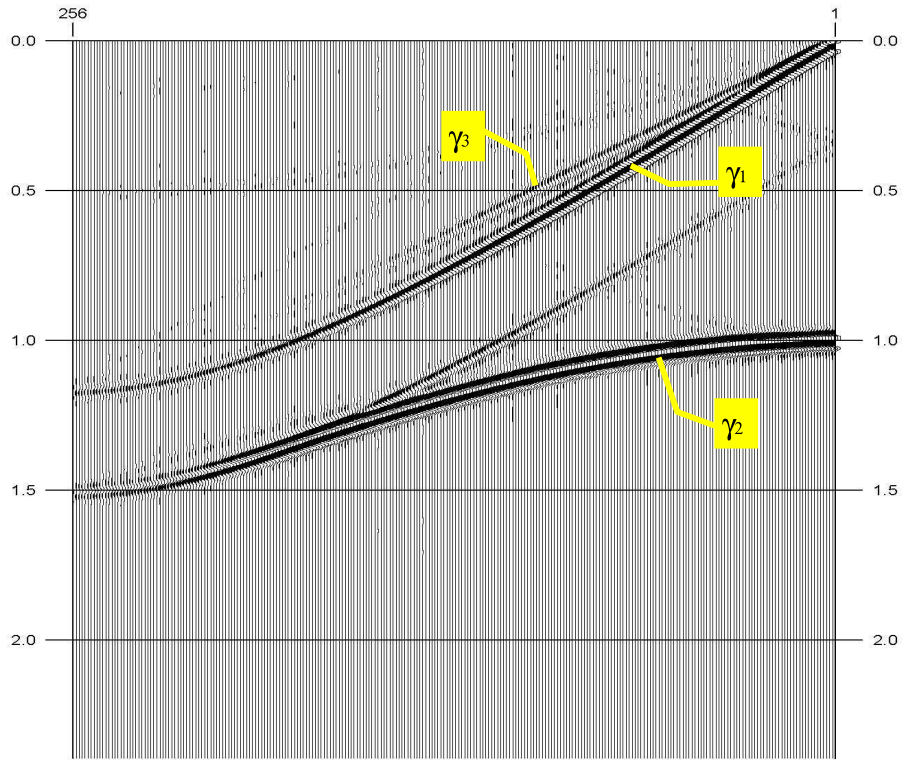

Figure 8. Cross-correlation of the pressure field with the particle velocity field constructs the field of virtual events: γ_1 represents autocorrelation of all the events; γ_2 represents cross-correlation of event α_2 with event β_1; and γ_3 represents cross-correlation of event α_3 with event β_1.

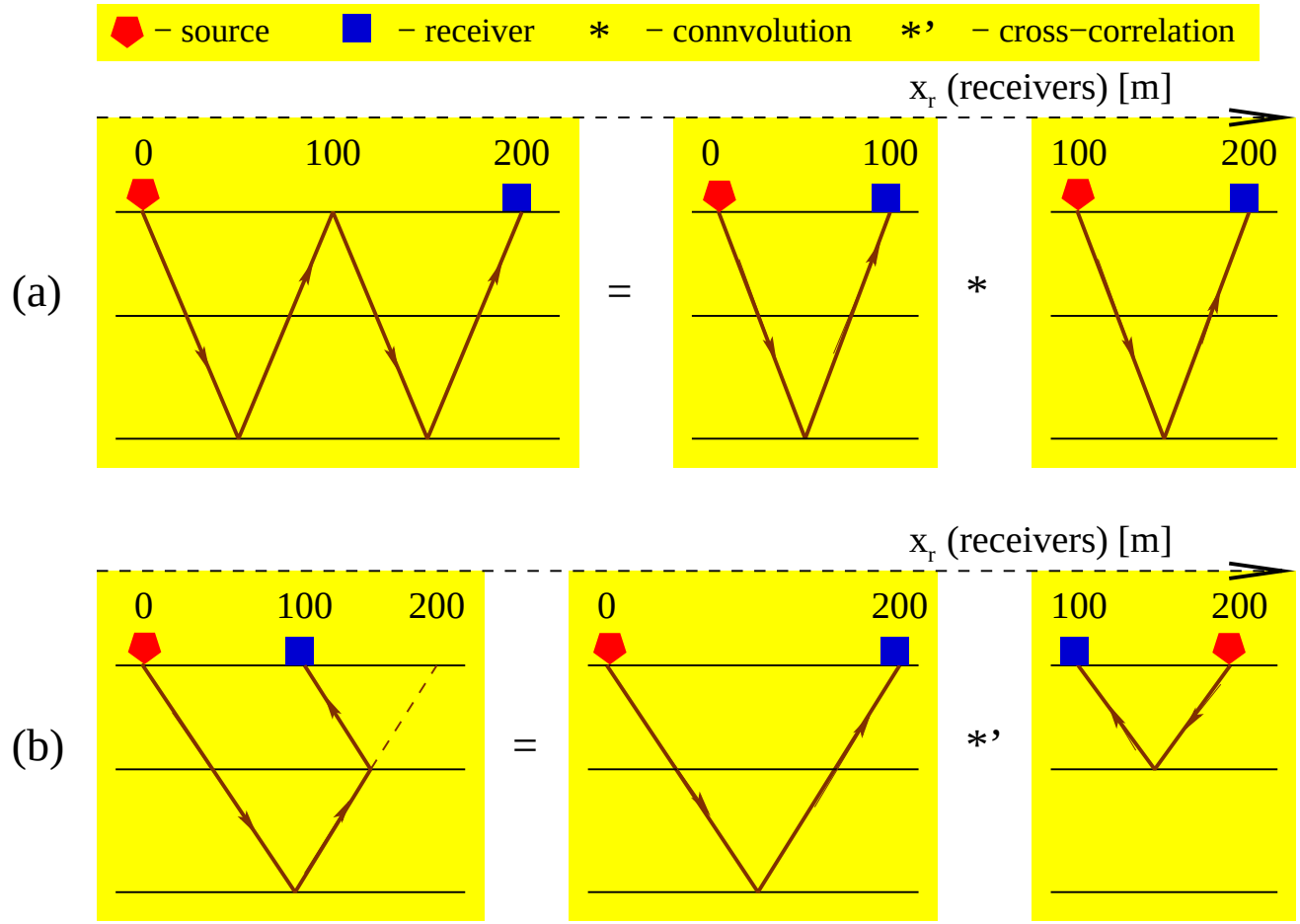

Figure 9. (a) - convolution extending offset from 100m to 200m, (b) - cross-correlation reducing offset from 200m to 100m.

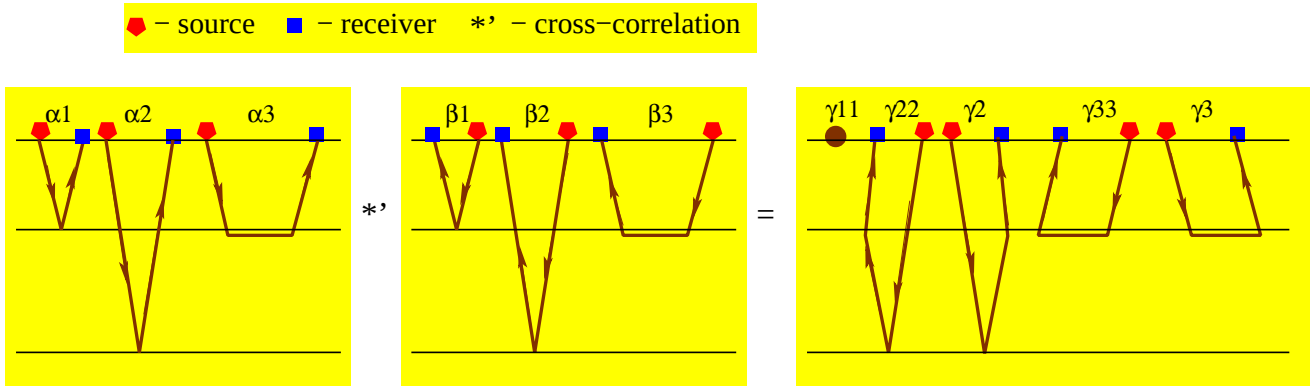

Figure 10. Creation of virtual field: cross-correlation of the data with itself creates 5 events: $\gamma_1 = \alpha_1\beta_1 + \alpha_2\beta_2 + \alpha_3\beta_3$ represents autocorrelation, $\gamma_{22} = \alpha_1\beta_2$ and $\gamma_2 = \alpha_2\beta_1$ represent cross-correlation of the first and second events and $\gamma_{33} = \alpha_1\beta_3$ and $\gamma_3 = \alpha_3\beta_1$ represent cross-correlation of the first and third events.

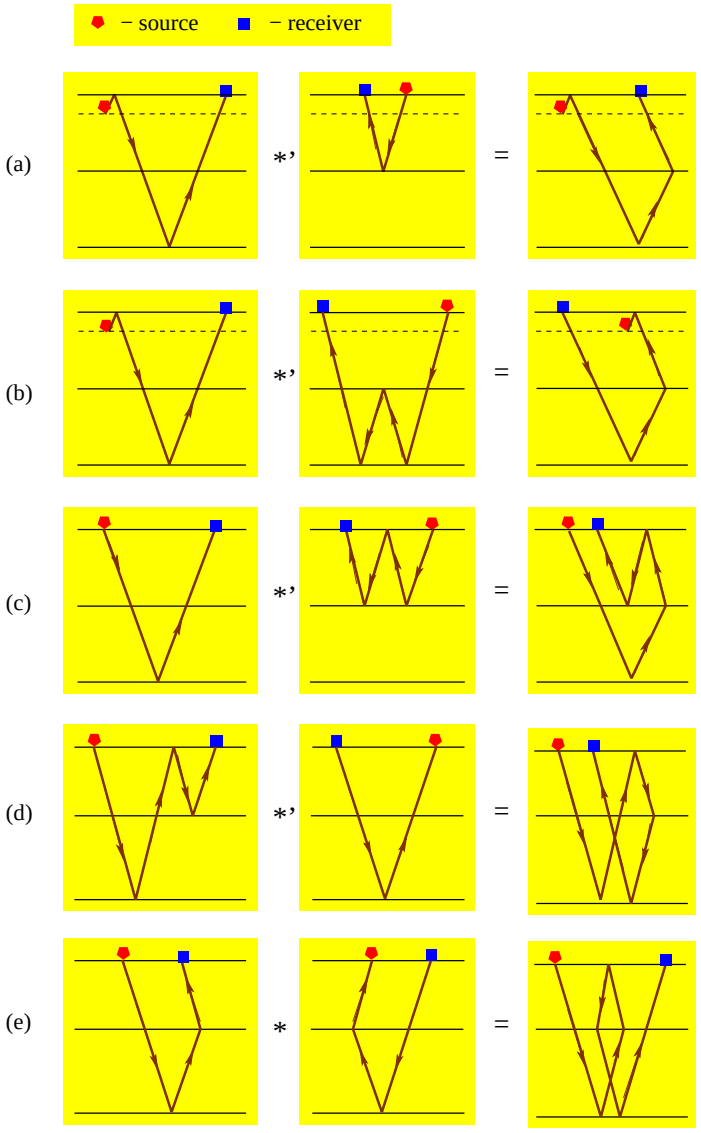

Figure 11. These scattering diagrams demonstrate potential applications of virtual event.

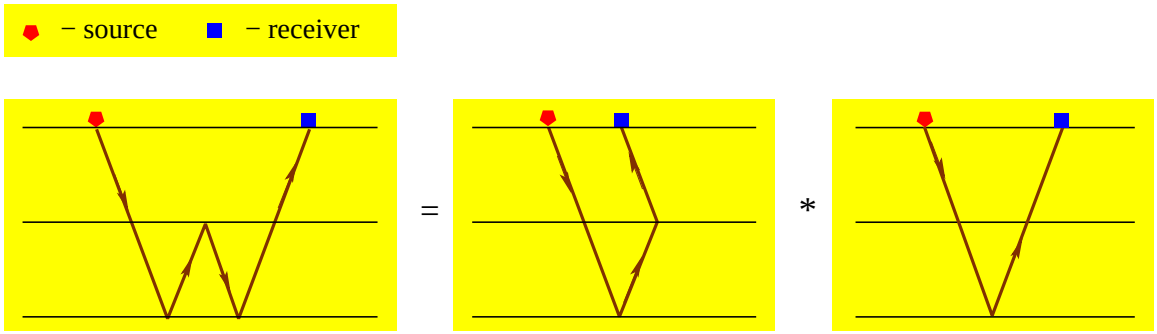

Figure 12. This scattering diagram demonstrates constructing internal multiple as application of virtual event for removing internal multiples.

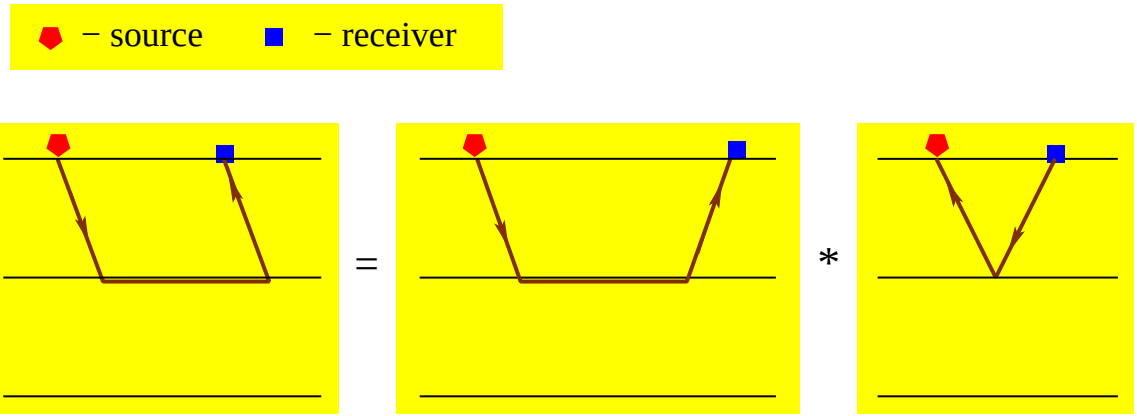

Figure 13. This scattering diagram demonstrates constructing refraction virtual event as application of virtual event for separating reflected and refracted waves.

CHAPTER II

PHYSICS OF SEISMIC VIRTUAL EVENT

The name of virtual events suggests that such events are not real–i.e., they do not exist. That is not true. In fact, we suggest that virtual events have a very important physical meaning in seismic analysis. Seismic virtual events have a real physical basis, and their roots are in the representation theorem; they follow physical laws and are created from real seismic events.

My goal in this chapter is to review the physical aspects of a virtual event. In the first section, I introduce physical interpretation of virtual events. In the second section, I discuss the relationship between the virtual events and the representation theorem. My objective in describing this relationship is to point out that virtual events obey basic physical laws, particularly Snell's law, which I discuss in the following section. The last section is the summary for the physical aspects of a virtual event.

1. Physical meaning of virtual events

To get more insight into virtual events let us imagine seismic acquisition that has a source and receivers on the interface I_1 above the second layer of the model in Figure 5. This model is shown in Figure 14 (b), alone with the model in Figure 5, which has now been renamed Figure 14 (a) to facilitate the comparison between the two models. Since we do not want to record free-surface reflections, the first layer of the model in Figure 14 (b) is not relevant. The model in Figure 14 (b) simulates the synthetic data shown in Figure 15 (a), and the model in Figure 14 (a) is the one related to the field of virtual events in Figure 15.

The claim is that the arrival time of reflection δ [Figure 15] coincides with the

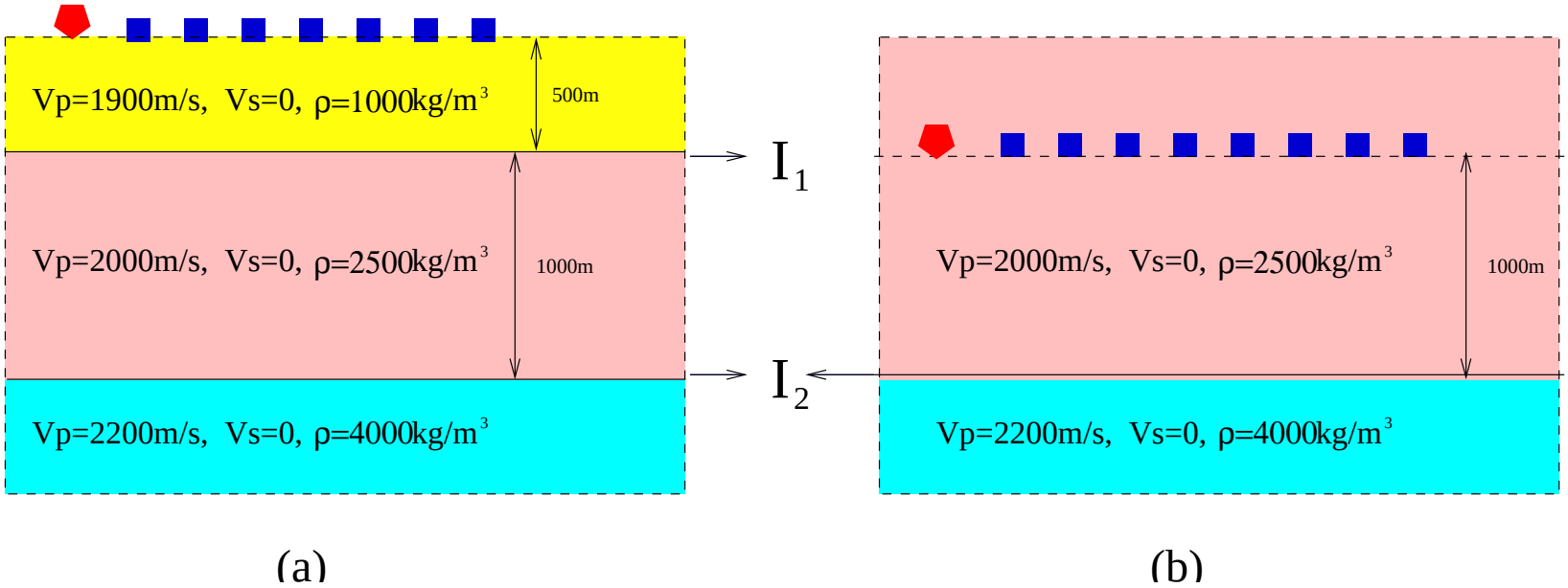

Figure 14. Two models: (a) - the model from the previous chapter is brought here for comparison; (b) - this model has the same relevant parameters as the previous model (i. e. thickness, velocities and densities of the second and third layers), with the source and the receivers on top of the second layer to test arrival times in the second layer only (we don't consider free-surface reflections, thus the first layer is not relevant).

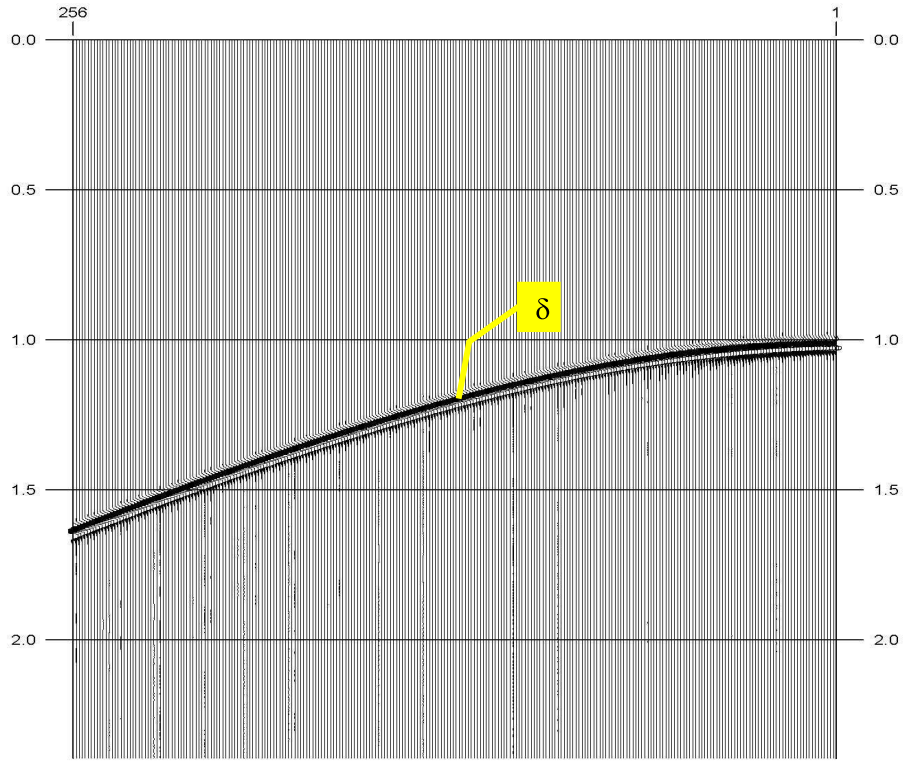

Figure 15. Synthetic data with one event α that represents time spent in the second layer only.

arrival time of virtual reflection γ_2 on Figure 8 (Note the difference in amplitudes; we compare the time arrival only and take care of the amplitude later.). In other words, virtual event represents the time a wave spent in second or/and lower layers only, depending on the scattering point of the second event in the real data (i.e., α_2 or β_2 - see Figures 8 and 10 for reference). So the time it takes for the wave to travel through the layers above is canceled out.

A virtual reflection gives us information about a single subsurface layer. In a way, we can think of it as a primary event corresponding to situation in which all layers above a specific one have been removed.

Let me illustrate this with an example in Figure 16 by comparing real and virtual primary reflections. Real events α_1, α_2, and α_3 propagate through the first layer, the first two layers, and the first three layers, respectively. The propagation times are always the sum of all the layers through which the signal had passed. Therefore, the propagation time through a single layer appears only in combination with the propagation times through the layers above, according to Snell's law.

The virtual primary reflections γ_1, γ_2, and γ_3, on the other hand, each give the propagation times through one or two subsurface layers. Namely, γ_1 corresponds to the propagation in the second layer only, γ_2 corresponds to the propagation in the third layer only, and γ_3 corresponds to the propagation in the second and the third layers. Virtual reflection γ_1 and γ_2, which represent each one layer only, are therefore treated on an equal footing with the first real primary α_1. They explicitly clarify two-way time spent in each layer separately.

Note that event γ_3 represents the time the wave spends in two layers together, therefore γ_3 'arrives' later than γ_1 and γ_2. Moreover, γ_2 might arrive before γ_1 if the second layer is no thicker than the first one, and the velocity increases with depth.

Unfortunately, event γ_3 and similar virtual events which correspond to more

than one layer, as well as virtual multiples, make correct identification of the one-layer virtual primaries difficult, because they look alike, just as real multiples can be confused with real primary reflections.

2. Virtual events in the representation theorem

Although these new events are virtual and theoretical, they actually are created by the representation theorem (Ikelle and Gangi, 2005). The representation theorem comes in two forms: the convolution form and the correlation form. The original derivations of the representation theorem were all in the convolution form (de Hoop, 1966, 1995; Gangi, 1970), until the recent derivations of the correlation form of the representation theorem were proposed by de Hoop (1966, 1995), Gangi (1970), and Bojarski (1983). The correlation form involves only real events, as opposed to the correlation form, whose use in seismology literature has been limited so far. It turns out that the correlation form is exactly what we are looking for when we are dealing with virtual events. The reason for it is hidden in its name: the correlation form of the representation theorem uses cross-correlation to produce its events, just like the method used to create virtual events that has been described above. Let us look closely at the equations to see exactly what makes one form of the theorem miss virtual events and the other type produce it.

The convolution form of the representation theorem is written as follows:

$$\begin{aligned} P_0(x_r,\omega,x_s) &= P_P(x_r,\omega,x_s) + \\ &+\frac{1}{s(\omega)}\oint_S dS(x)\sigma(x)\mathbf{n}\Big[P_P(x,\omega,x_r)\frac{\partial P_0(x,\omega,x_s)}{\partial \mathbf{n}} - \\ &-P_0(x,\omega,x_s)\frac{\partial P_P(x,\omega,x_r)}{\partial \mathbf{n}}\Big], \end{aligned} \tag{2.1}$$

where P_0 denotes recorded data in the frequency domain, P_P denotes data in the frequency domain that contains only primaries and internal multiples, ω is a frequency, x_r indicates receiver locations, x_s indicates source locations, and σ is the inverse of density. S represents the surface of integration, which consists of two parts: S_0 is the free surface, and S_R represents a hemisphere of radius R. An illustration of the model with these surfaces is given in Figure 17. The convolution form of the representation theorem produces free-surface multiples, but not virtual events, because it deals only with causal fields: P_0 and P_P are both forwardgoing events.

The correlation form of the representation theorem is written as follows:

$$\begin{aligned} s^*(\omega)P_0(x_r,\omega,x_s) \quad & +s(\omega)P_P^*(x_r,\omega,x_s) = \\ & = \oint_S dS(x)\sigma(x)\mathbf{n}\Big[P_P^*(x,\omega,x_r)\frac{\partial P_0(x,\omega,x_s)}{\partial \mathbf{n}} - \\ & \quad -P_0(x,\omega,x_s)\frac{\partial P_P^*(x,\omega,x_r)}{\partial \mathbf{n}}\Big], \end{aligned} \tag{2.2}$$

where the asterisk $*$ refers to the complex conjugate in the frequency domain. This form of the representation theorem uses crosscorrelation instead of convolution. Thus the second field in the equation (2.2) is a complex conjugate. So the first field is going forward in time, and the second one is going backward in time (be cause it is a complex conjugate of P_P), creating good conditions for producing virtual events along with real ones, and combining forward and backward propagation in one event.

However, it is the same theorem, thus it is supposed to give the same solution, no matter which form we use. What does make virtual events in the correlation form of the representation theorem disappear in the final outcome?

Let us look at the integral over surface S, which is called the Kirchhoff scattering integral. When performing the Kirchhoff integral in the convolution form of the

representation theorem (2.1), we will see that only the free surface contributes to the integral in equation (2.1). According to Sommerfeld's radiation condition (Sommerfeld, 1954), if R goes to infinity, surface S_R goes to zero. Using the model in Figure 17 as an example, we separately computed the Kirchhoff scattering integral over surfaces S_0 and S_R, i.e., the integral over the surface S_0, as follows:

$$\sigma \int_{S_0} dS\Big[P_P \frac{\partial P_0}{\partial z} - P_0 \frac{\partial P_P}{\partial z}\Big], \tag{2.3}$$

and the integral over surface S_R as follows:

$$\sigma \int_{S_R} dS\mathbf{n}\Big[P_P \frac{\partial P_0}{\partial \mathbf{n}} - P_0 \frac{\partial P_P}{\partial \mathbf{n}}\Big]. \tag{2.4}$$

Figure 18 presents the results of these computations. It shows that the integral in (2.4) is effectively negligible; it is of the order 10^{-7}, whereas the integral in (2.3) is of the order 1.

Using the same model as in the previous example (Figure 17), we again computed the Kirchhoff scattering integral, this time in the correlation form of the representation theorem (2.1) over surfaces S_0 and S_R, as follows, respectively:

$$\sigma \int_{S_0} dS\Big[P_P^* \frac{\partial P_0}{\partial z} - P_0 \frac{\partial P_P^*}{\partial z}\Big], \tag{2.5}$$

and

$$\sigma \int_{S_R} dS\mathbf{n}\Big[P_P^* \frac{\partial P_0}{\partial \mathbf{n}} - P_0 \frac{\partial P_P^*}{\partial \mathbf{n}}\Big]. \tag{2.6}$$

The results of these integrations are depicted in Figure 19. The values of the integral in (2.5) and the integral in (2.6) are of the same order in this case and clearly cannot be neglected. Also note that we have now received negative time.

The difference between the Kirchhoff integrals in (2.3) & (2.4) and (2.5) & (2.6) occurs because in the correlation form of the representation theorem the second field

is time-reversed: the propagation starts at infinity ($R \longrightarrow \infty$), and it decays toward the source, which causes Sommerfeld's radiation condition to fail in this case.

Knowing that both forms of the representation theorem have to produce the same final result, let us compare the Kirchhoff integral over S_0 in both cases, i.e., we compare the result of the integral in (2.3) in Figure 18 (a) (for convenience, this algorithm is called 'ConvInt' throughout the rest of this chapter), and the result of the integral in (2.5) in Figure 19 (a) (I will call it 'CorrInt' for the same reason). Remember that the wavelets will not look totally identical because we are looking at only part of equations (2.1) and (2.2); this small difference in wavelets is also due to the face that convolution expands data, whereas crosscorrelation compresses data. Therefore events on ConvInt come with delay with respect to the events on CorrInt. The figures have common time in the range from $t = 0$ to $t = 1s$. In this range ConvInt has three events: the first one starts at $t = 0.1s$, the second starts at $t = 0.7s$, and the third starts at $t = 1.0s$. With good approximation we can identify the first event on ConvInt as the same event that starts at $t = 0$ on CorrInt, the second event on ConvInt as the event that starts at $t = 0.6s$ on CorrInt, and the third event on ConvInt as the event that starts at $t = 0.9s$ on CorrInt. These are the real events in this range on CorrInt; all others should be virtual.

To be certain of this conclusion, let us again examine the two Kirchhoff integrals of the correlation form of the representation theorem in (2.5) and (2.6). Each one has two members that depend on an outgoing normal vector, $\mathbf{n}$. Some of the events related to the integral in (2.5) and some of the events related to the integral in (2.6) are identical, but they have the opposite sign. These are virtual events. They cancel each other out during the calculation, so we do not see them in the outcome. For example, look at the virtual event on CorrInt that begins at $t = 0.1s$. It has a symmetrical event on the figure below (the integral over S_R) at the same time, so

that when we sum these two integrals, the two virtual events will be canceled out.

To summarize, the two forms of the representation theorem produce the same result but in different ways. The correlation form produces virtual events that are canceled out in the process of the Kirchhoff integration and does not make it to the final result.

3. Following Snell's law

At first sight, these new backgoing virtual events seem to violate Snell's law of ray-paths. For example, think of water or light waves in real life. When you point your flashlight on the lake floor at some angle θ_1, as suggested in Figure 20, you expect to see spot b, knowing that the light ray passes through the lake surface and continues its movement at angle θ_2. You would be very surprised to discover that your flashlight is lighting up spot a and the light ray is bent the "wrong" way at angle $-\theta_2$. However, that is exactly what "virtual life" would be like if we compare light rays to virtual events.

But virtual events are derived from the representation theorem, therefore, like anything that is consistent with the representation theorem, they should obey physical laws. And actually, such a "wrong-bending" situation has been studied in optics (Houck et al., 2003). Optic ray bends the "wrong" way in a specially created kind of materials, generally known as left-handed materials (LHM). LHM are artificial materials which are created in the laboratory and have a negative refraction index, as opposed to the positive refraction index of the right-handed materials (RHM). LHM cause ray to bend the "wrong" way, just like virtual events in seismics coming up from scattering point.

The major difference between optic and seismic cases is that optics deals with

a single interface, whereas seismics is forced to deal with at least two – the reflector and the refractor. So seismic wave going down behaves as it does in RHM, but going up behaves as it does in LHM. Therefore, in order to measure these virtual waves, the optic solution is a one-step solution – finding or creating LHM and using it in a regular experiment; while seismic solution is built of two steps – finding or creating the LHM equivalent and performing an acquisition that would take care of this dual behavior. Since a material, that behaves RHM in one direction and LHM in the other direction, has not been discovered yet, virtual events cannot be recorded by any measurement device. In the laboratory, however, we can solve one step in the problem by suggesting a two-part experiment and the following model.

The dual behavior would not be a problem if source and receivers are placed on the different sides of the seismic model, as demonstrated in Figure 21. The first model [Figure 21 (a)] is made of two seismic equivalents of RHM; it has the source on top of the first layer and the receivers on the bottom of the second layer. The recorded wave would represent the down-going part of the virtual event. The second model [Figure 21 (b)] is made of the lower RHM equivalent with the same parameters as the lower RHM in the first model, and upper LHM equivalent with almost all the parameters as the upper RHM on the first model, except for the quantity which is responsible for the material being left-handed. The receivers are now on the top of the first layer, as in regular acquisition. However, the source is on the bottom of the second layer and is no longer a point-source. It is a front-source which is the recorded wave from the first model. The second part of the experiment is building the upgoing part of the virtual event. The wave recorded by the receivers in the second model will represent the virtual event itself. That way we can eliminate one step of the measuring problem. However, the other one is still unsolved. The problem, therefore, is to create seismic equivalent of the left-handed material in the laboratory, that has

not been done yet.

In conclusion, although we can construct virtual events from data, virtual events cannot be recorded today. But it is important to remember, that virtual fields are in complete consistency with Snell's law.

4. Conclusions

In this chapter we proposed a physical interpretation of seismic virtual events, they cancel the influence of the upper layers on the time the wave propagates in the subsurface. Virtual events provide additional information on the subsurface structure, as they represent time a wave spent in a single subsurface layer.

Also we stated that according to Ikelle and Gangi (2005) virtual events are produced by the representation theorem. Solving the correlation form of the representation theorem instead of the convolution form, virtual events appear and cancel each other out so that in the outcome only real events are left.

Seismic virtual events obey generalized version of Snell's law, in analogy with light in optics, which behave similarly in left-handed materials.

In conclusion of this chapter, virtual events are legitime physical events that have concrete physical meaning, produced by the representation theorem, therefore obey physical laws.

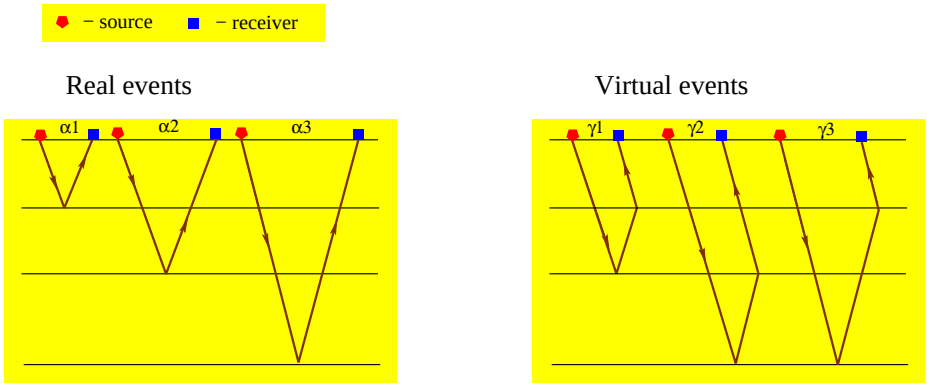

Figure 16. Real and virtual primary reflections in three layer model.

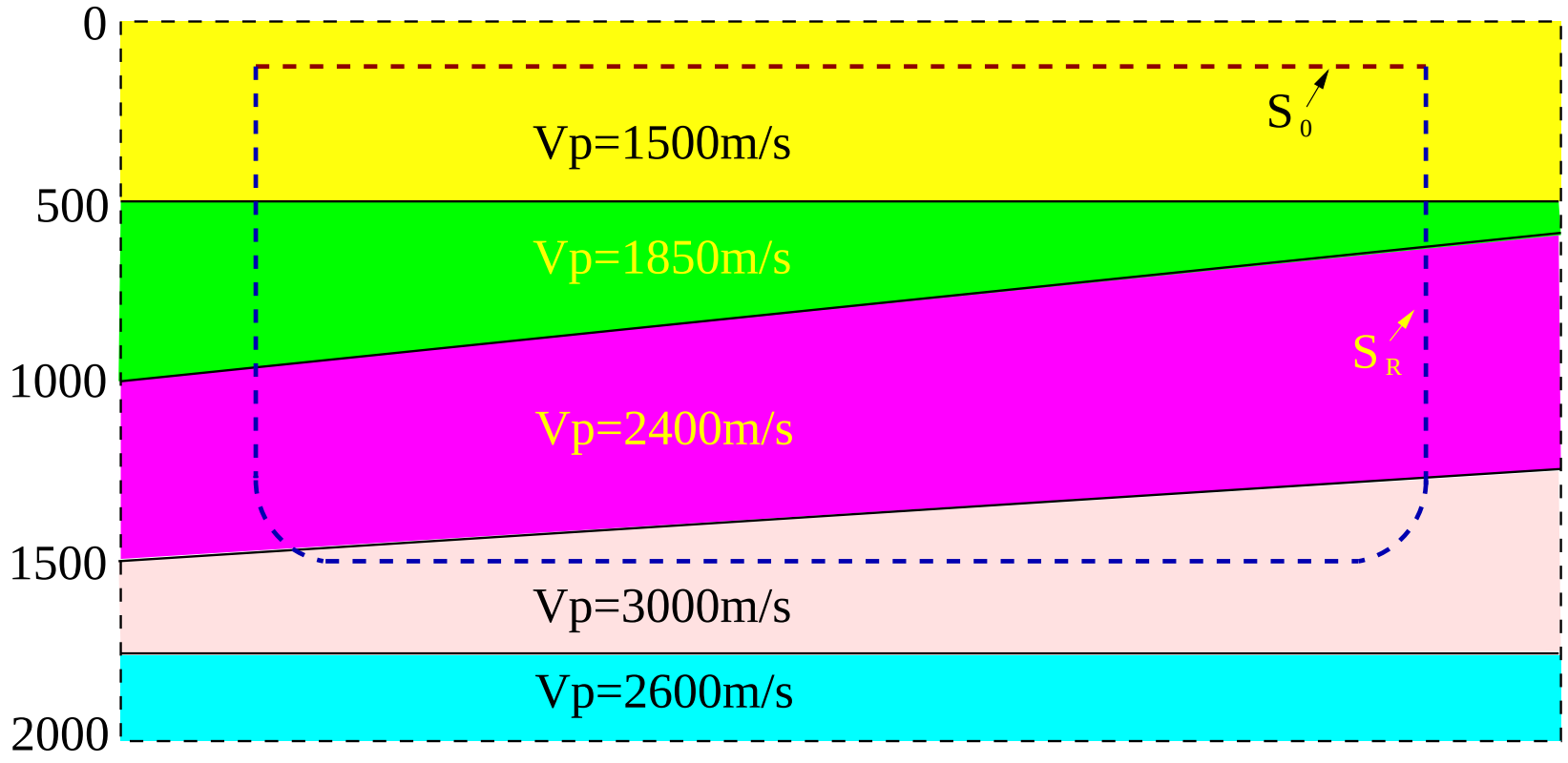

Figure 17. The model is built to simulate the data that would demonstrate the difference between integration in two forms of the representation theorem.

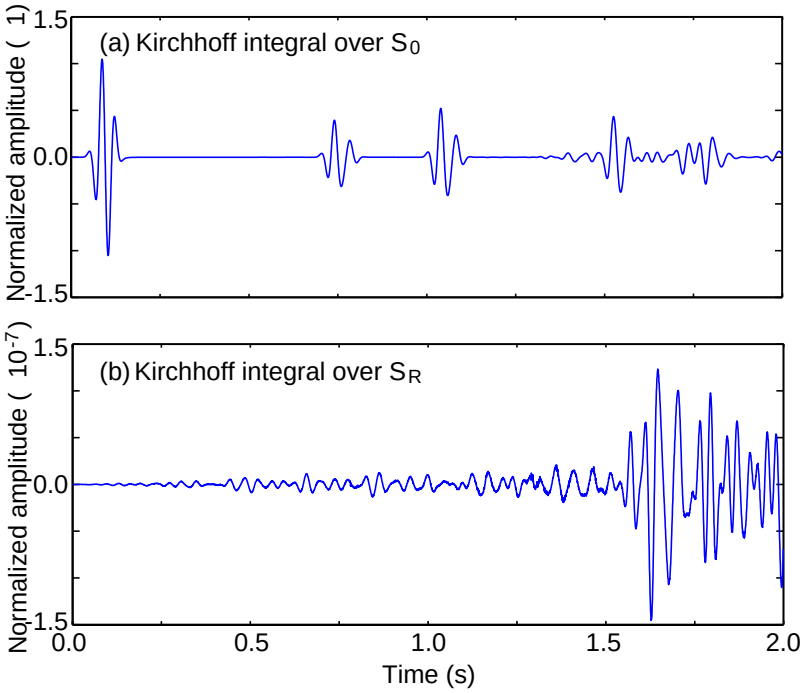

Figure 18. Integration over the surface S_R (b) of the model according to the convolution form of the representation theorem shows negligible values comparing to the integration over the free surface S_0 (a).

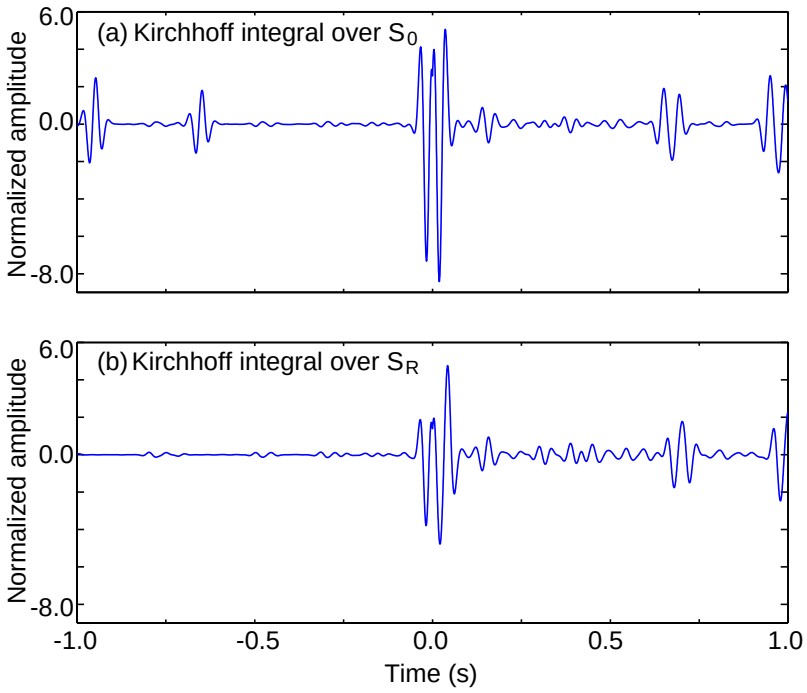

Figure 19. Integration over the surface S_R (b) of the model according to the correlation form of the representation theorem shows the same order of values as in the integration over the free surface S_0 (a).

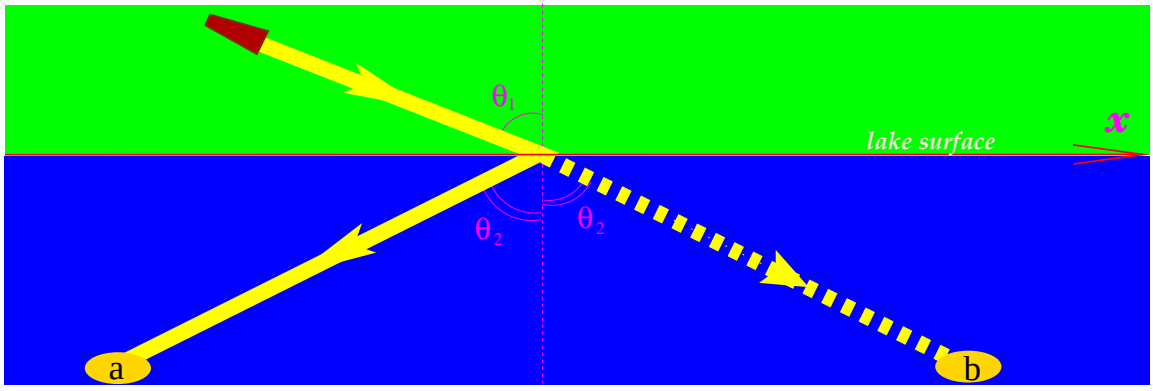

Figure 20. Light ray behavior as if it was virtual event: it is bending the "wrong" way, when passing from air to the water of lake.

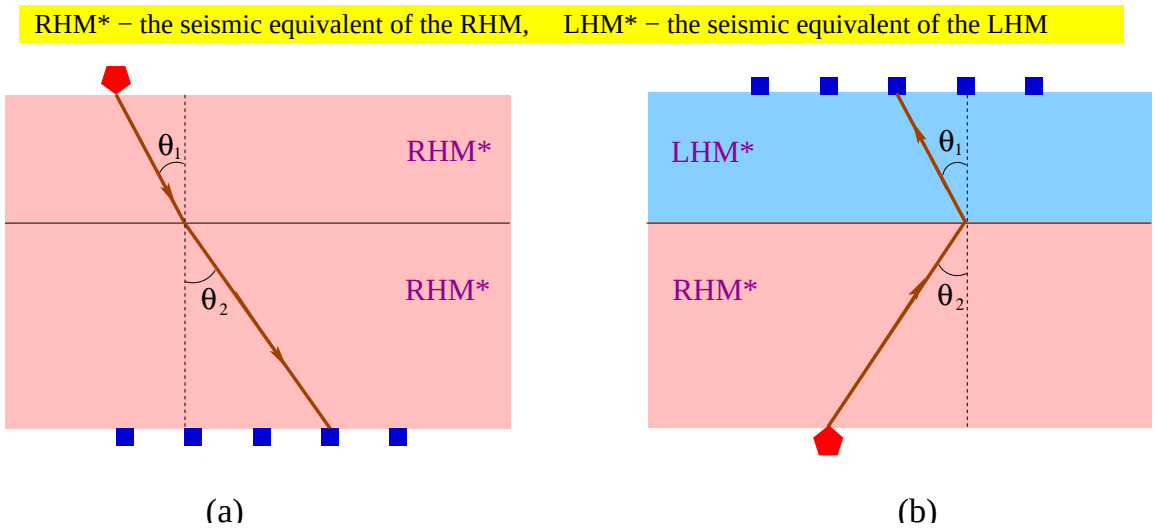

Figure 21. Possible way to record virtual events under the condition of existing of seismic equivalent of the LHM in two-part experiment involving two models: (a) - both materials are RHM, the source is on the top and the receivers are on the bottom, (b) - the model is almost identical to the model (a), except for the quantity of the upper material that makes it LHM, with the receivers on top and the front-source on the bottom.

CHAPTER III

VIRTUAL EVENTS IN ATTENUATION OF INTERNAL MULTIPLES

In seismic acquisition, along with useful primaries, we record unwanted events such as multiples. While there are many techniques for attenuating free-surface multiples [e.g. predictive deconvolution, CMP stacking, F-K filtering, Radon transform, inverse scattering multiple attenuation (ISMA), demultiple based on the Kirchhoff or Born scattering theory], there is very little we can find about internal multiples [Hansen (1948), Robinson (1957), and Schneider et al. (1965) used the predictive deconvolution for internal multiple attenuation, which holds up only for a 1D medium; Berkhout and Verschuur (1997) developed a feedback method that requires the selection of the multiple generating reflector of the velocity model of the subsurface; Jakubowicz (1998) based his diagrams on the downgoing continuation proposed by Berkhout and Verschuur (1997), and Weglein et al. (1997) used the inverse scattering series, which is very expensive and requires all frequencies for the computation of an internal multiple at a given frequency].

Free-surface multiples have at least one scattering point on the free surface, which facilitates the formulations of the free-surface multiple attenuation. The scattering points at the free surface are obtained for receivers and source near the free surface.

Internal multiples have no scattering points at the free surface. All the scattering points of the internal multiples are inside the subsurface structure, which is unknown, and therefore the free-surface attenuation approach cannot readily be extended to the attenuation of internal multiples.

With the introduction of the concept of virtual events, which brings information about the subsurface structure to the free surface, we can retrieve information about the scattering points of internal multiples, and solve the problem of internal-multiple

attenuation. In fact, we can use existing techniques for the attenuation of free-surface multiples, modified in such a way that the combination of virtual events with real events will predict internal multiples.

This chapter is organized as follows. In the next section, I will review the mathematical descriptions of multidimensional convolution and crosscorrelation. In the second section, I will also review the basic concept of the free-surface multiple attenuation, which is useful for my internal multiple attenuation. In the third section, I will describe my strategy for attenuation of internal multiples. My discussion in this chapter focuses on marine towed-streamer data. However, i will explain how my strategy for internal multiple attenuation can be adopted to OBS data.

1. Convolution and crosscorrelation

Because multidimensional convolution and crosscorrelation play a key role in this chapter, allow me to define first these operators. Let $f_1(t)$ and $g_1(t)$ be one-dimensional functions in the time domain, and $f_1(\omega)$ and $g_1(\omega)$ will be the Fourier transform of $f_1(t)$ and $g_1(t)$, respectively. Then the one-dimensional convolution between them is written as follows ($\times$ is a notation for one-dimensional convolution):

$$CV_1(t) = f_1(t) \times g_1(t) = \int_{-\infty}^{+\infty} f_1(t')g_1(t-t')dt'$$

The Fourier transform of $CV_1(t)$ is denoted by $CV_1(\omega)$ and the convolution becomes simple multiplication:

$$CV_1(\omega) = f_1(\omega)g_1(\omega)$$

Now let $f_2(x,t)$ and $g_2(x,t)$ be multidimensional functions in time domain, and $f_2(x,\omega)$ and $g_2(x,\omega)$ will be the Fourier transform of $f_2(x,t)$ and $g_2(x,t)$ with respect to time, respectively. In this case the multidimensional convolution between

these functions is ($*$ is a notation for multidimensional convolution):

$$CV_2(t) = f_2(x,t) * g_2(x,t) = \int_{-\infty}^{+\infty} dx' \int_{-\infty}^{+\infty} dt' f_2(x',t') g_2(x', t-t')$$

The Fourier transform of $CV_2(t)$, denoted by $CV_2(\omega)$, is:

$$CV_2(\omega) = \int_{-\infty}^{+\infty} dx' f_2(x',\omega) g_2(x',\omega)$$

Since most of the time my data depend on three variables, e.g. x_r, x_s and ω, I want the multidimensional convolution to depend on the same three variables. Therefore the above formula will change as follows in the time domain and the Fourier domain, respectively:

$$CV_2(x_r, x_s, t) = \int_{-\infty}^{+\infty} dx' \int_{-\infty}^{+\infty} dt' f_2(x', x_s, t') g_2(x_r, x', t-t')$$

$$CV_2(x_r, x_s, \omega) = \int_{-\infty}^{+\infty} dx' f_2(x', x_s, \omega) g_2(x_r, x', \omega) \tag{3.1}$$

For that matter, multidimensional crosscorrelation which I will use later to construct virtual events, is written as follows, using the same logic as with multidimensional convolution in the time domain and the Fourier domain, respectively ($*'$ is a notation for multidimensional crosscorrelation):

$$CC(x_r, x_s, t) = f_2(x_r, x_s, t) *' g_2(x_r, x_s, t) = \int_{-\infty}^{+\infty} dx' \int_{-\infty}^{+\infty} dt' f_2(x', x_s, t') g_2(x_r, x', t'-t)$$

$$CC(x_r, x_s, \omega) = \int_{-\infty}^{+\infty} dx' f_2(x', x_s, \omega) g_2^*(x_r, x', \omega) \tag{3.2}$$

where asterisk $*$ denotes a complex conjugate.

2. Predicting free-surface multiples

This section will prepare us for the attenuation of internal multiples by introducing the following three important concepts:

1. why the formulation of the multiple attenuation technique is facilitated when we have the scattering point at the free surface;

2. what a BMG (bottom-multiple generator) reflector is and what role it plays in multiple attenuation; and

3. how the multidimensional convolution in (3.1) works with the data.

The mathematical and computational operations invoked in my construction of internal multiples are similar to those encountered in the construction of free-surface multiples based on the Kirchhoff or Born scattering theory [Ikelle and Amundsen (1997), Ikelle *et al.* (2003)]. When attenuating free-surface multiples, the data set is convolved with itself according to the Kirchhoff series. In a similar way for internal multiple attenuation, we perform a multidimensional convolution of the data with the field of virtual events, after we use the multidimensional crosscorrelation of pressure data with particle velocity data to receive the field of virtual events.

The BMG reflector is introduced by Ikelle and Amundsen (2002) to facilitate the calculations of predicting free-surface multiples. We use the same concept of the BMG reflector for internal multiple attenuation, with one difference: this time it is not just to speed the process. Rather, it is necessary, as we will see later.

Note, that sometimes I use word 'predict' instead of 'construct'. These words have exactly the same meaning. I use 'prediction' when I refer to multiples for historical reasons only: the literature of multiple attenuation uses the first term rather than the other.

Allow me to introduce the technique for attenuation of free-surface multiples, which I am going to combine with virtual events later in order to attenuate internal multiples.

A. The benefit of the scattering point at the free surface

Let us denote towed-streamer data which contain no direct waves as $\mathbf{\Phi_0} = [P_0, V_0]^\top$, where P_0 is the pressure data (measured by a hydrophone), and V_0 is the vertical component of particle velocity (measured by a geophone). To remove free-surface multiples, the following nonlinear equation is used [Ikelle *et al.*, 2003]:

$$\mathbf{\Phi_P} = \mathbf{\Phi_0} - a\mathbf{\Phi_1} + a^2\mathbf{\Phi_2} - a^3\mathbf{\Phi_3} + \cdots, \tag{3.3}$$

where

$$\mathbf{\Phi_{n+1}} = \mathbf{\Phi_n} * V_0$$

and where $\mathbf{\Phi_P}$ is data without free-surface multiples and a is an inverse source signature.

The first term of the series is $\mathbf{\Phi_0}$ – the original data as it is. The second term is: $a\mathbf{\Phi_1} = a\mathbf{\Phi_0} * V_0$, which means that the original data are convolved with V_0, scaled with factor a. Let me show how the multidimensional convolution works in this second term and how it takes advantage of the scattering point at the free surface to construct free-surface multiples.

Figure 22[1] shows the convolution between two sets of events of the same data. In terms of wave propagation, the process is just a combination of the wave-propagation paths of different events. In other words, the receiver point of one event connects

[1]The figures in this subsection do not include arrows, because there is no backward wave propagation in the free-surface-multiple attenuation.

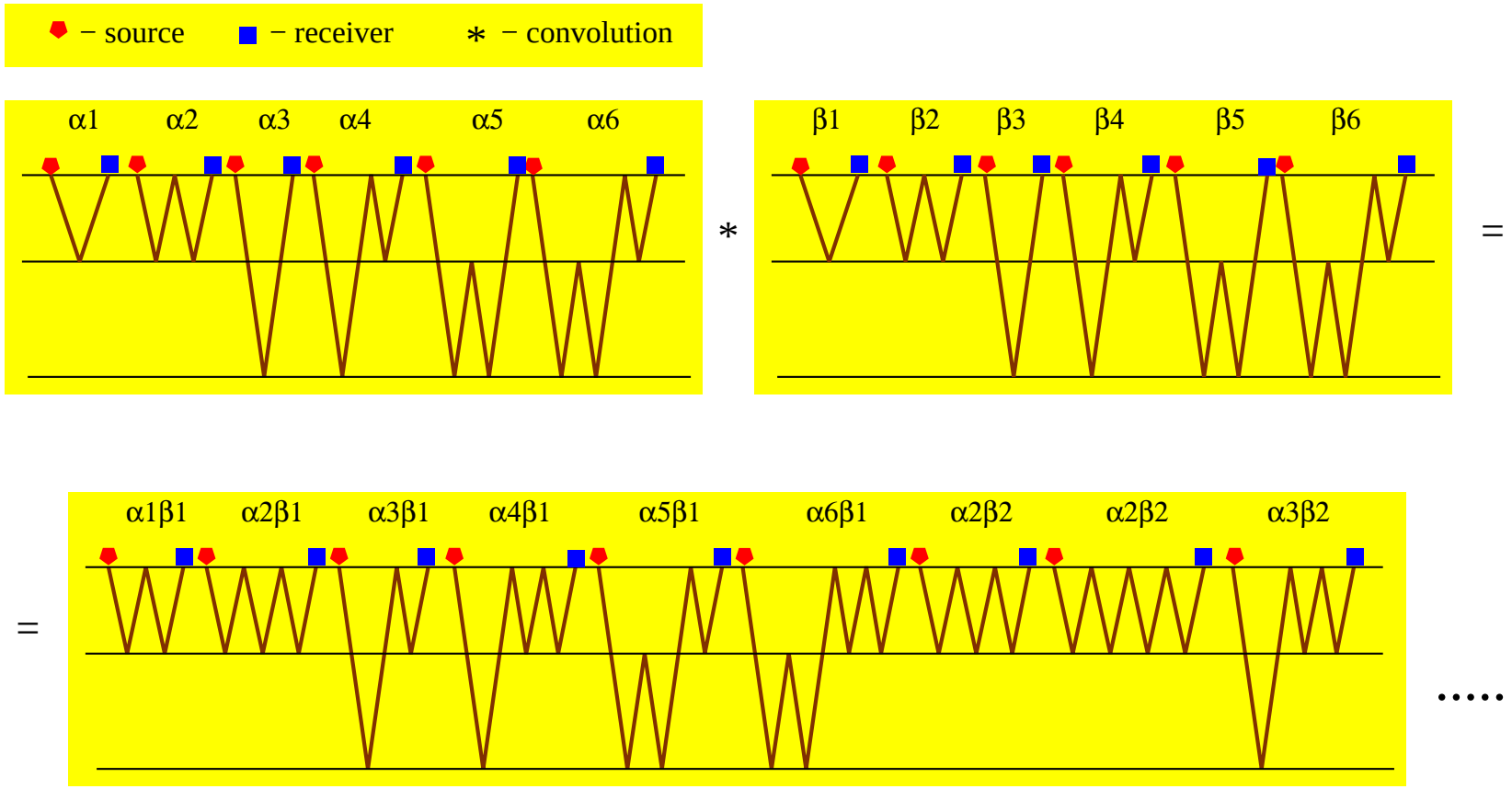

Figure 22. Convolution of data with itself makes a long row of free-surface multiples.

with the source point of another event, they become one and constitute a scattering point of the newly created event. Since all the receivers and sources in the towed-streamer data are near the free surface[2], the result of the convolution in the second term of the Kirchhoff series contains many different and sometimes repeated free-surface multiples. No primaries, or internal multiples, are constructed, since they do not bounce at the free surface. So in the first two terms of the series (3.3), we are actually subtracting free-surface multiples from the data.

Let us understand now why we need the other terms of equation (3.3). As I mentioned earlier, some of the multiples are predicted twice or more. Figure 23 demonstrates different ways to construct free-surface multiples. Those that have one bounce at the free-surface (first-order free-surface multiples) are predicted only once (Figure 23a), but those that have two bounces at the free-surface (second-order free-surface multiples) are predicted twice, because there are two ways to construct them (Figure 23b). There are three ways to construct third-order free-surface multiples (Figure 23c); therefore these multiples are predicted three times, and so on. So by taking first two terms of the equation (3.3), we remove first-order free-surface multiples, and remove one set of all other free-surface multiples, leaving one set of second-order, two sets of third-order free-surface multiples, and so on. Higher order terms in Kirchhoff series take care of residuals of higher-order multiple.

The third term of the equation (3.3) is $a^2(\mathbf{\Phi_1} * V_0)$. In a similar way as before, this convolution constructs free-surface multiples, but this time one set of second-order, two sets of third-order, three sets of fourth-order ets., because all the events of Φ_1 bounce at the free surface at least one time (all of them are free-surface multiples). The inverse source signature takes care of the reduced amplitude. In other words, the

[2]In real applications, the wave is extrapolated to the free surface, which is not a problem, since the velocity of the water is known.

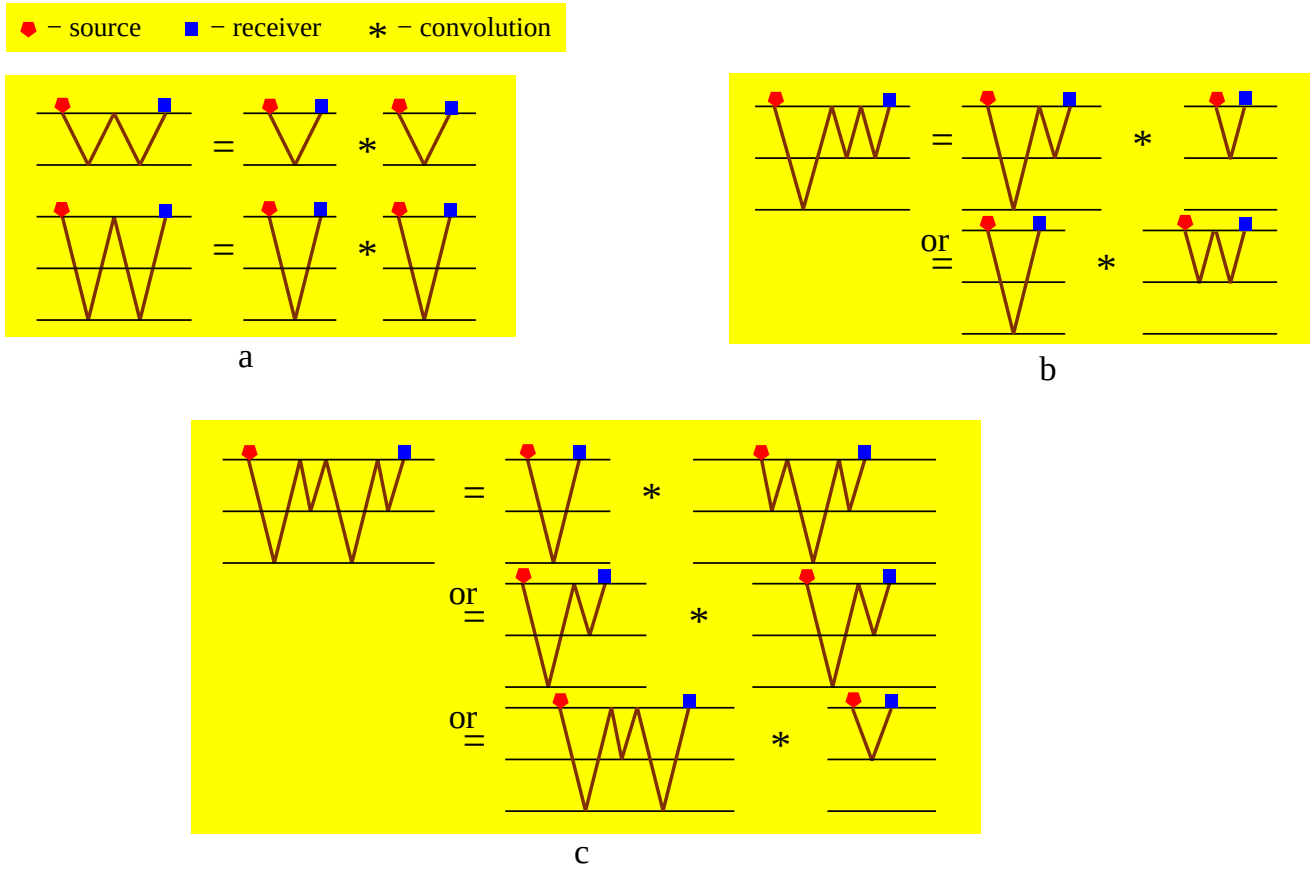

Figure 23. There is only one way to construct free-surface multiples with one bounce at the free-surface (a), there are two ways to construct multiples with two bounces (b), and three ways for the ones with three bounces (c).

third term of the series removes second-order free-surface multiples. Similarly, the fourth term of the equation removes third-order free-surface multiples, and so on.

When trying to attenuate internal multiples, we so not have direct access to the scattering point, since it is not at the free surface anymore. But we use the same idea in internal-multiple attenuation when convolving the data with the virtual field.

However, this approach for the attenuation of free-surface multiples is not convenient, since it is nonlinear. Ikelle et al. (2004) developed a linear approach for the same attenuation technique, which is called the bottom-multiple generator (BMG) approach.

B. The BMG reflector

To describe the linear solution for the problem of multiple attenuation, bottom-multiple generator (BMG) reflector must be introduced. But before I describe its use, let me clarify its purpose. The BMG reflector in the free-surface multiple attenuation technique is supposed to facilitate the calculations, make the technique work faster. By contrast, in the internal multiple attenuation technique, the BMG approach is a necessity, a tool that the attenuation technique would not work without.

The BMG reflector is a hypothetical reflector. The arrival times of the primary associated with its reflector coincides with the arrival time of the first water-bottom multiple. In other words, the data above this hypothetical primary consist of primary and internal multiple reflections only. It allows us to create data that contains only primaries and internal multiples by muting the data below the BMG reflection, including the BMG reflection, leaving the data that are above the first water-bottom multiple (which is only primaries and internal multiples). These primaries and internal multiples are convolved with the entire data. By removing multiples from one set of the data before the multidimensional convolution, we avoid predicting some

multiples several times, and the problem becomes linear.

Using the BMG reflector, the solution of the free-surface multiple attenuation comes in two steps. In the first step, the data that contain only primaries and internal multiples ($\mathbf{\Phi_0^a} = [P_0^a, V_0^a]^\top$) takes the place of the particle velocity data in the original series. For the first step, equation (3.3) will be replaced by the following linear equation:

$$\mathbf{\Phi_{pa}} = \mathbf{\Phi_0} + a\mathbf{\Phi_{1a}}, \tag{3.4}$$

where

$$\mathbf{\Phi_{1a}} = \mathbf{\Phi_0^a} * V_0$$

In this case, $\mathbf{\Phi_{1a}}$ predicts all the orders of free-surface multiples, and it predicts them only once. However, it does not predict free-surface multiples whose first bounce is located below the BMG reflector. That is why in the second step we define a portion of the demultipled in the first step data, $\mathbf{\Phi_{pa}}$, which contains only data below the BMG reflection, and we denote it $\mathbf{\Phi_{pa}^b}$. Next we convolve $\mathbf{\Phi_{pa}^b}$ with the vertical component of the particle velocity of the 'primaries' data, V_0^a, and the convolution is denoted by $\mathbf{\Phi_{1b}}$:

$$\mathbf{\Phi_{pb}} = \mathbf{\Phi_{pa}} + a\mathbf{\Phi_{1b}}, \tag{3.5}$$

where

$$\mathbf{\Phi_{1b}} = \mathbf{\Phi_{pa}^b} * V_0^a$$

Once again, the term $\mathbf{\Phi_{1b}}$ predicts free-surface multiples only once. But this time it predicts only free-surface multiples, that have their last bounce on the first reflector. It does not predict again the events with the first bounce above the first BMG reflector, as they have been removed in the first iteration in $\mathbf{\Phi_{pa}}$.

Now we are left only with the multiples that have both the first and last bounce

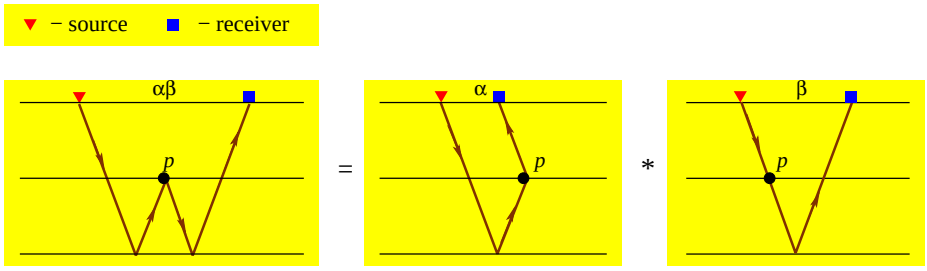

Figure 24. Internal multiples can be constructed by convolution of a virtual event with a real event.

below the BMG reflection. In deep-water acquisitions these multiples are barely visible and do not require special treatment. In cases where these multiples need attenuation, the BMG reflector location will be moved lower, and the data will be divided again.

This approach is used in internal-multiple attenuation (we call it the BIMG approach), because the division of data is necessary in order to avoid constructing primaries. I will return to this point later on.

3. Basic approach for attenuating internal multiples

When constructing free-surface multiples, multidimensional convolution is performed on two sets of the same data. When dealing with internal multiples, one of the two data sets is the field of virtual events. Assume that we have seismic data free of direct waves and free-surface reflections. The data consist of the pressure field $P(x_r, x_s, \omega)$, recorded by hydrophones, and the vertical component of the particle velocity $V(x_r, x_s, \omega)$, recorded by geophones for the receiver at x_r, for the source point at x_s and for frequency ω. $P_v(x_r, x_s, \omega)$ denotes the pressure field of virtual events, and $P_m(x_r, x_s, \omega)$ denotes the pressure field of internal multiples. The construction

of the internal multiples is done by the following multidimensional convolution:

$$P_m(x_r, x_s, \omega) = \int_{-\infty}^{+\infty} dx P_v(x, x_r, \omega) V_0(x, x_s, \omega) \tag{3.6}$$

Figure 24 explains equation (3.6) with scattering diagrams and shows the construction of an internal multiple that can be made from the free surface. We combine the wave-propagation paths of two events that have a common point on the free surface at the receiver point of the first event and the source point of the second event. Event β is a primary reflection, and event α is a virtual reflection, one that does not exist in the seismic record. As we described in the previous chapter, we have to create this virtual reflection by a multidimensional crosscorrelation of pressure data and particle velocity data. This multidimensional crosscorrelation is written as follows:

$$P_v(x_r, x_s, \omega) = \int_{-\infty}^{+\infty} dx P^*(x_r, x, \omega) V(x, x_s, \omega) \tag{3.7}$$

and as before, where the asterisk $*$ denotes a complex conjugate. The complex conjugate of $P(x_r, x_s, t)$ in the frequency domain (i.e., $P^*(x_r, x_s, \omega)$) means $P(x_r, x_s, -t)$ in the time domain; in other words, the events in data set P propagate backward. As a result, the events in the virtual field combine both forward and backward wave propagation. This fact allows us to cancel out the legs in Figure 24 of virtual event α and primary β in Figure 24 from point P up to the surface (according to the arrows).

The combination of (3.6) and (3.7) allows us to predict internal multiples, just as free-surface multiples are predicted in the Kirchhoff series. Actually this combination can also create primaries and direct waves, which we want to avoid creating in the context of internal multiple attenuation. For this reason we have developed the following strategy:

1. **Division** of the data into two fields, A and B;

2. Construction of the **virtual field** using the multidimensional crosscorrelation of A with B [Figure 23];

3. Prediction of **internal multiples** using the convolution of the virtual field with B [Figure 24];

4. **Subtraction** of the constructed internal multiples from the original data;

5. Demultiple of **second-order** internal multiples; and

6. Repeat the procedure with a different division, when necessary.

I will expand each of the four steps in the next subsections.

A. Step 1: Bottom Internal Multiple Generator

Unlike free-surface multiple construction, the process of constructing internal multiples can generate primaries as well. For instance, Figure 25 shows two examples of constructing primaries by combining equations (3.6) and (3.7). Each example consists of two steps: the multidimensional convolution and the multidimensional crosscorrelation. The first example [Figure 25 (a)] shows the creation of such a virtual field in the first step, which contains a virtual direct wave (combined autocorrelation of each event, I will expand on virtual direct wave in the next section). The next step predicts all the data that have been convolved with this virtual field, including primaries. The second example [Figure 25 (b)] shows the construction of the virtual field in the first step, but the convolution with the first primary generates another primary in the next step.

To avoid this outcome, the original data should be divided (step one) in two data fields [$P_a(x_r, x_s, \omega)$ and $P_b(x_r, x_s, \omega)$, $V_a(x_r, x_s, \omega)$ and $V_b(x_r, x_s, \omega)$] prior to virtual

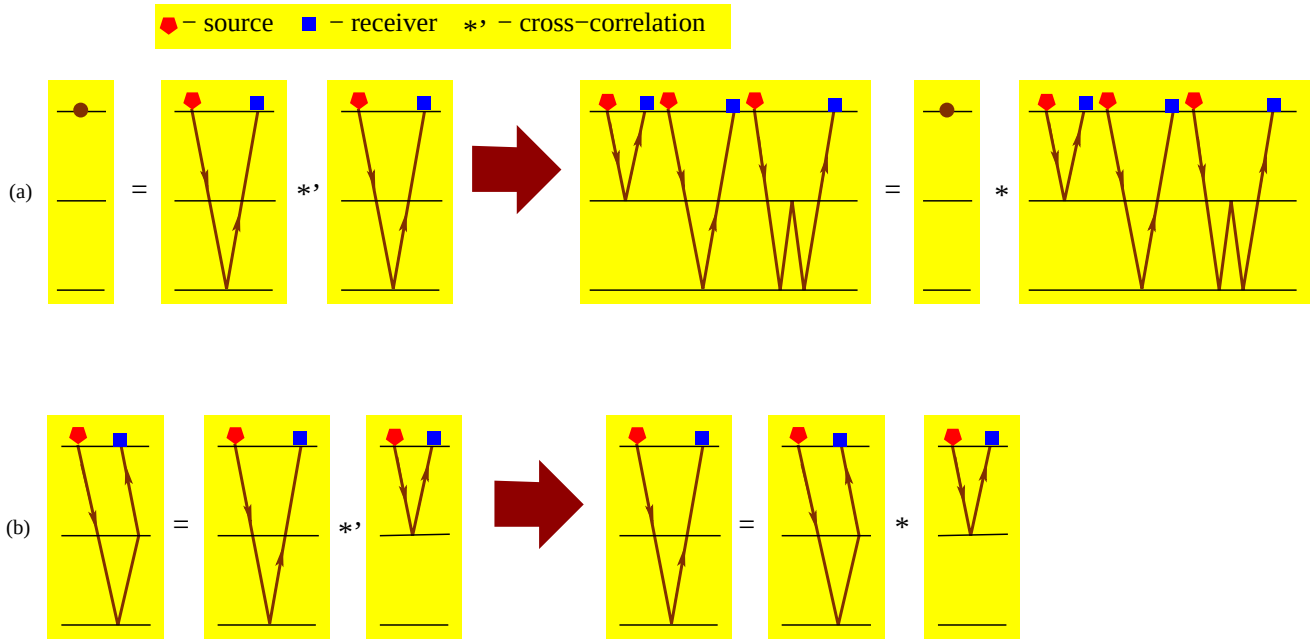

Figure 25. Two examples of constructing primaries.

field construction. To do so we use the concept of bottom internal multiple generator (BIMG) reflector – a hypothetical reflector. The arrival times of the primary associated with its reflector coincides with the arrival time of the first internal multiple. This is a paraphrase of the idea of the bottom-multiple-generator reflector in free-surface multiple attenuation [Ikelle et al. (2004), Watts and Ikelle (2006)]. And in this case the BIMG approach is not just optimization. We use it for a different objective than the BMG approach in free-surface-multiple attenuation.

We apply the BIMG division before the multidimensional crosscorrelation (3.7) to construct virtual events related to a specific interface, i.e. bringing information about this interface, and predicting internal multiples with the first scattering point at this interface. This approach attenuates first-order internal multiples. However, unlike free-surface multiples, internal multiples are weaker to begin with, so higher-order internal multiples are barely constitute a problem.

Dividing the data at the BIMG reflection means that if there are more than one internal multiple generator in the data, we will use an iterative process to remove all internal multiples from the data. After predicting and subtracting one set of internal multiples in the first iteration, the demultipled second part of the data ($P_b(x_r, x_s, \omega)$, $V_b(x_r, x_s, \omega)$) are divided at a new BIMG location to predict and subtract another set of internal multiples.

An example is the simple 1D acoustic model presented in Figure 26. It generates two primary reflections, α_1 and α_2, and two internal multiples, μ_1 and μ_2, shown in Figure 27 on a seismogram and in Figure 30(a) in scattering diagrams. The first BIMG reflector is located just below primary α_1 and above primary α_2, creating two data sets: $P_a(x_r, x_s, \omega)$ [Figure 28 and Figure 30(b)] and $P_b(x_r, x_s, \omega)$ [Figure 29 and Figure 30(c)] (the same applies to the particle velocity data). This division will construct events related to the first interface, since the first set contains only primary

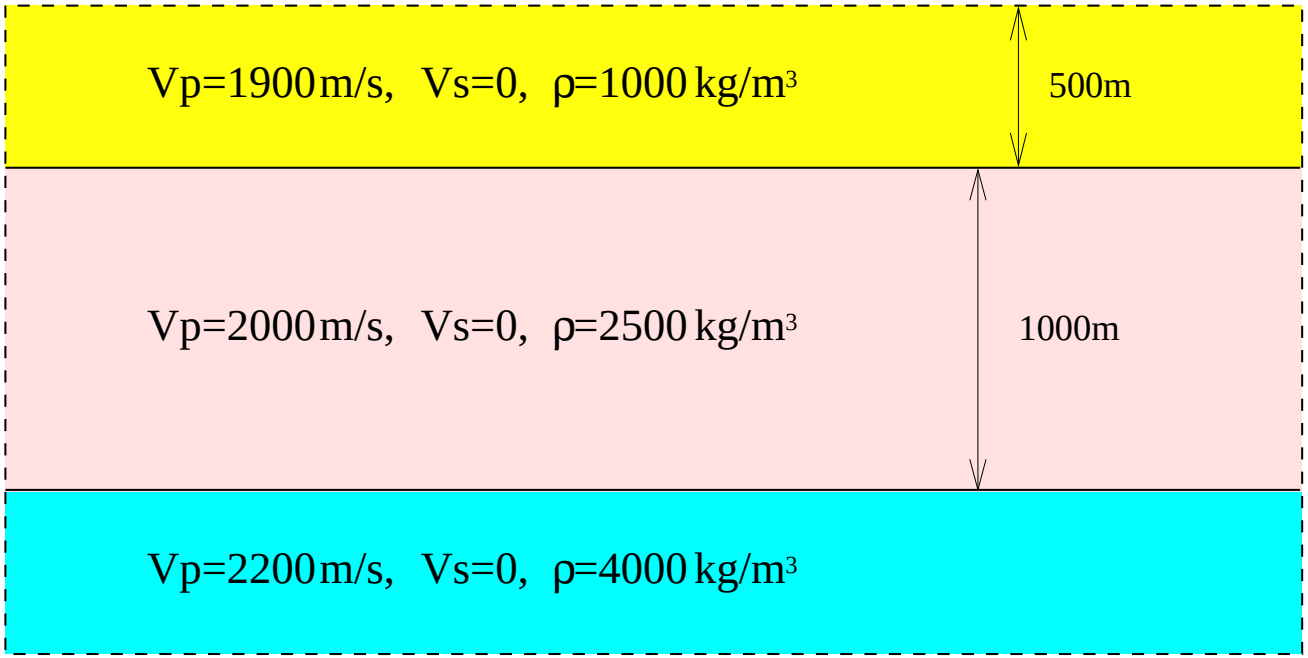

Figure 26. 1D acoustic model.

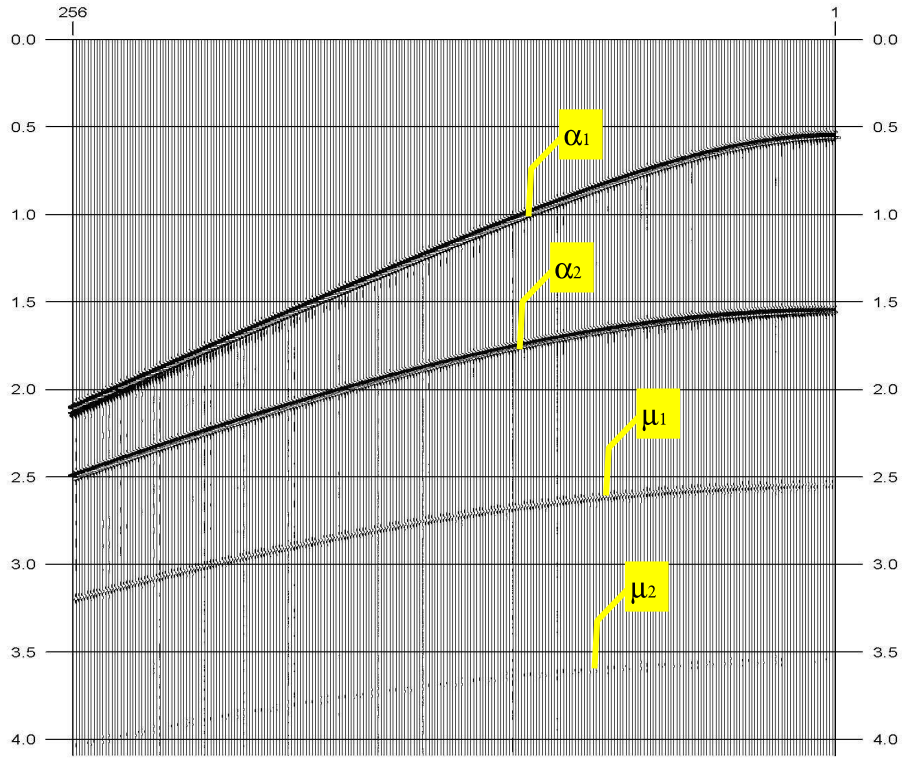

Figure 27. Pressure data generated by 1D model shows two primary reflections.

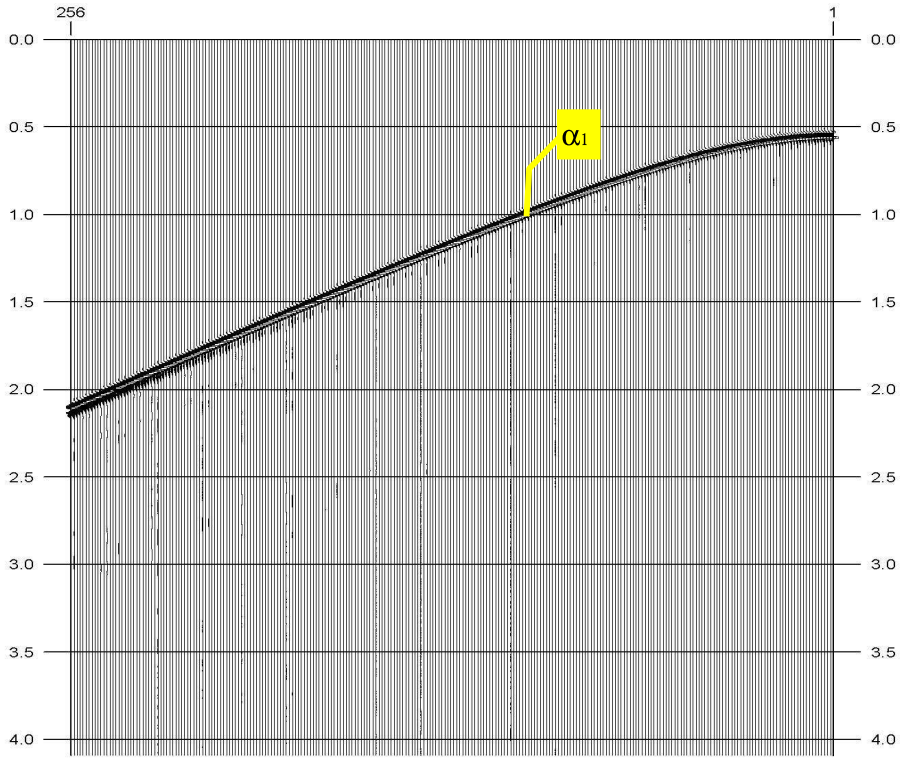

Figure 28. Pressure data: first data set after applying the concept of BIMG.

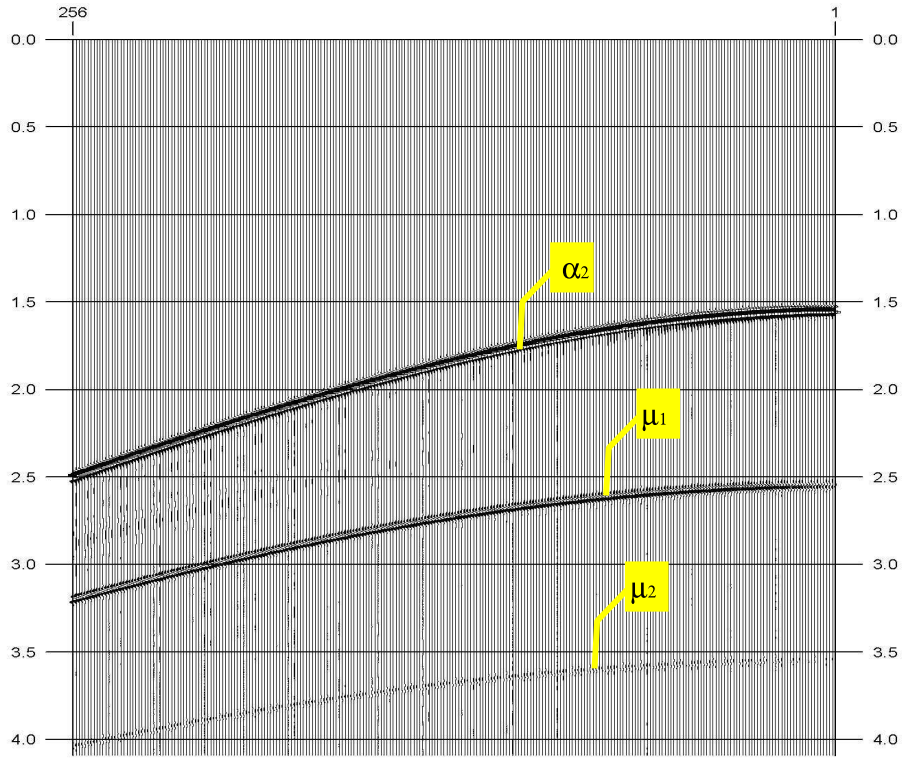

Figure 29. Pressure data: second data set after applying the concept of BIMG

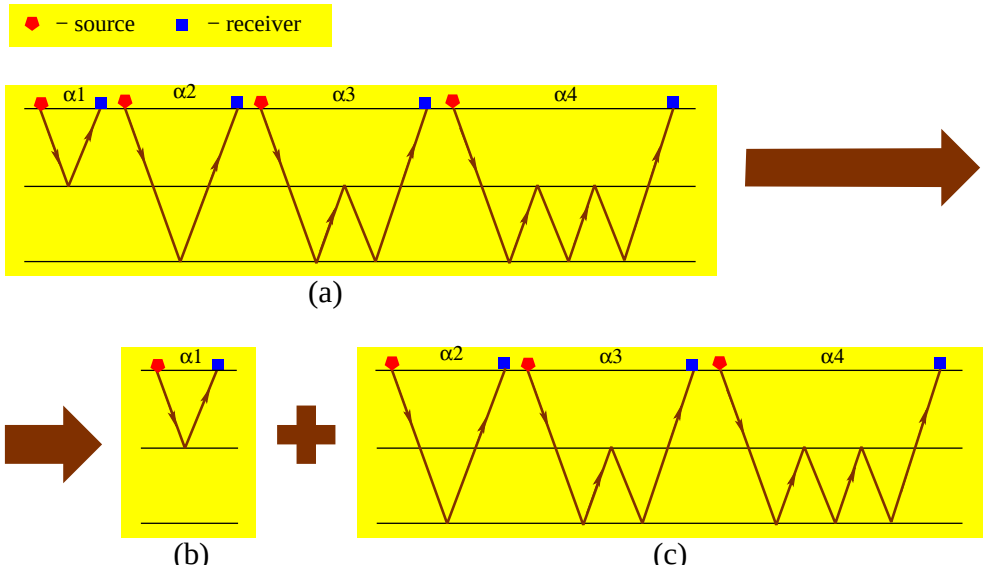

Figure 30. Scattering diagrams of the data and their division at BIMG location.

α_1. After prediction and subtraction of one set of multiples, the BIMG is located in the demultipled second set below the primary α_2, creating data set P_{2a}, which contains only primary α_2, and data set P_{2b}, that contains all the events below α_2, and so on.

B. Step 2: Construction of virtual events

Virtual events are constructed by the multidimensional crosscorrelation of two sets of data, as was described in Chapter I. The same scattering diagram is valid here [Figure 23]. But for the attenuation of internal multiples, we should not use the same events in both data sets, as was mentioned previously, to avoid creation of the virtual direct wave (autocorrelation) to prevent the creation of primaries. In the previous example, data set $P_a(x_r, x_s, \omega)$ contains only one primary α_1. The data set $V_b(x_r, x_s, \omega)$ does not include this primary, but the original data $V(x_r, x_s, \omega)$ does. Let us compare two virtual fields: one from the multidimensional crosscorrelation of $P_a(x_r, x_s, \omega)$ with $V(x_r, x_s, \omega)$, depicted in Figure 31(a) on scattering diagrams and Figure 32 on seismogram, and one from the crosscorrelation of $P_a(x_r, x_s, \omega)$ with $V_b(x_r, x_s, \omega)$, depicted in Figure 31(b) on scattering diagrams and Figure 33 on seismogram. The only difference between these two is the crosscorrelation of event α_1 with itself, i.e., autocorrelation of event α_1. The seismograms differ only in regard to the virtual direct wave γ_1: Figure 32 has it, but Figure 33 does not. Thus in the process of the attenuation of internal multiples, we do not use the raw data but rather the data after applying BIMG. Therefore, equation (3.7) becomes

$$P_v(x_r, x_s, \omega) = \int_{-\infty}^{+\infty} dx P_a^*(x_r, x, \omega) V_b(x, x_s, \omega). \tag{3.8}$$

It is important to take the complex conjugate of the data set that contains the early arrivals which is in this case P_a, and not the other one, as the complex

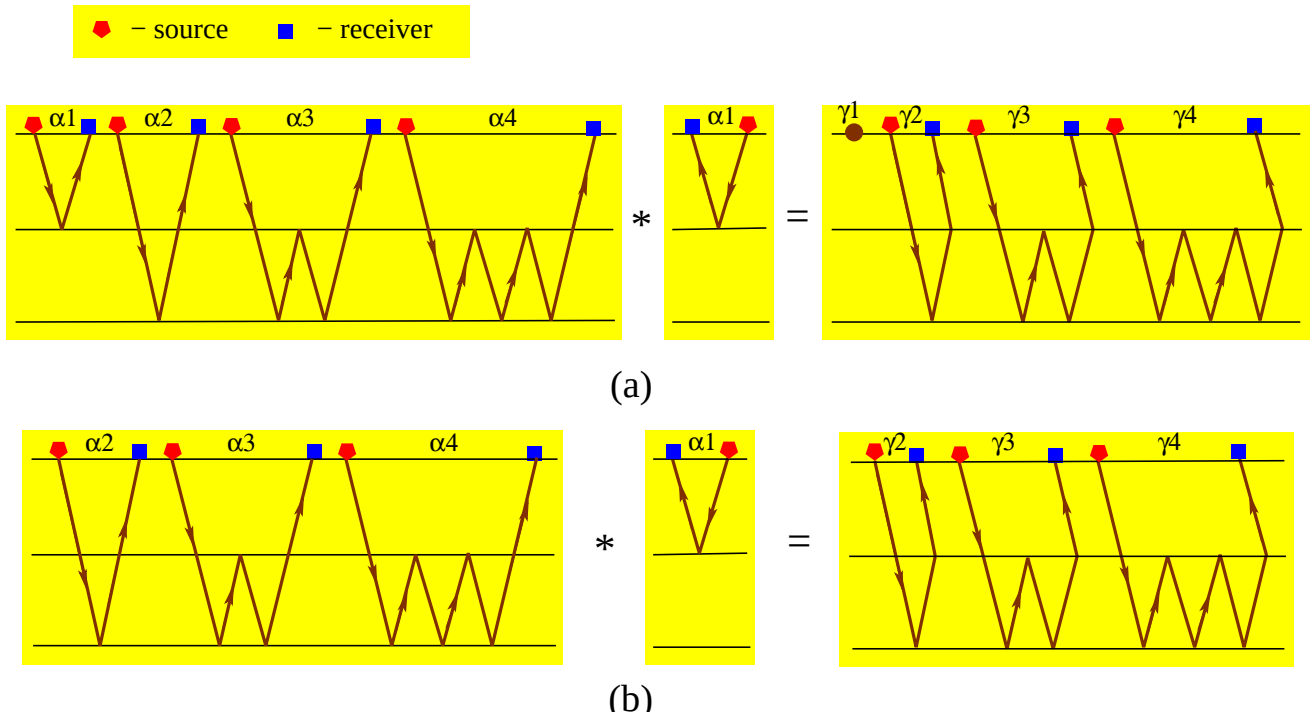

Figure 31. Scattering diagrams of construction of virtual events.

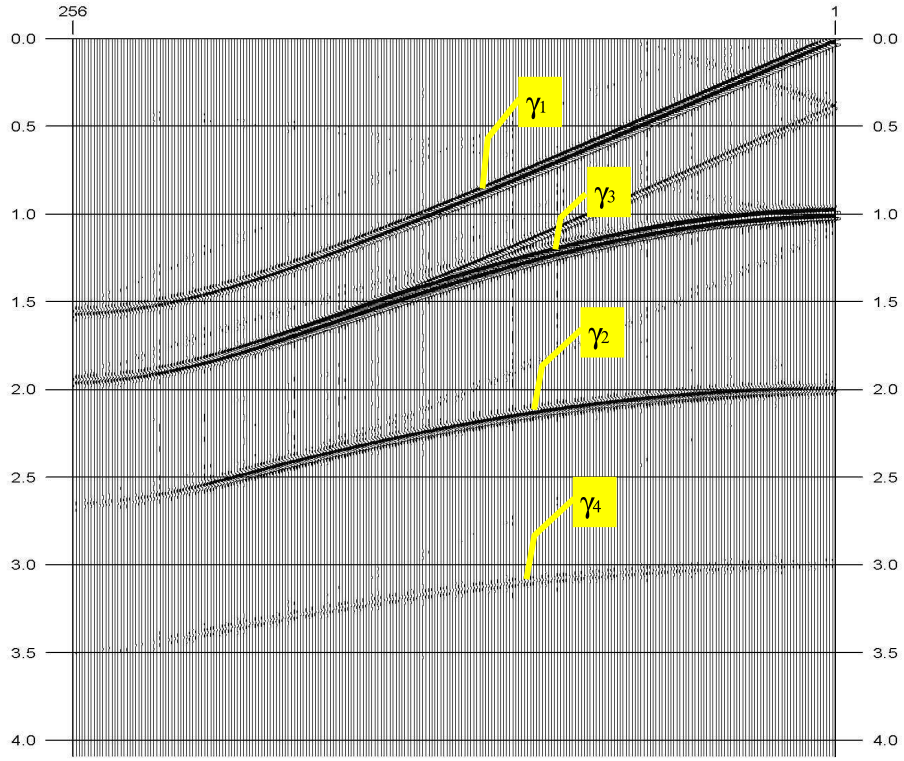

Figure 32. Virtual field constructed by multidimensional crosscorrelation of $P_a(x_r, x_s, \omega)$ with $V(x_r, x_s, \omega)$.

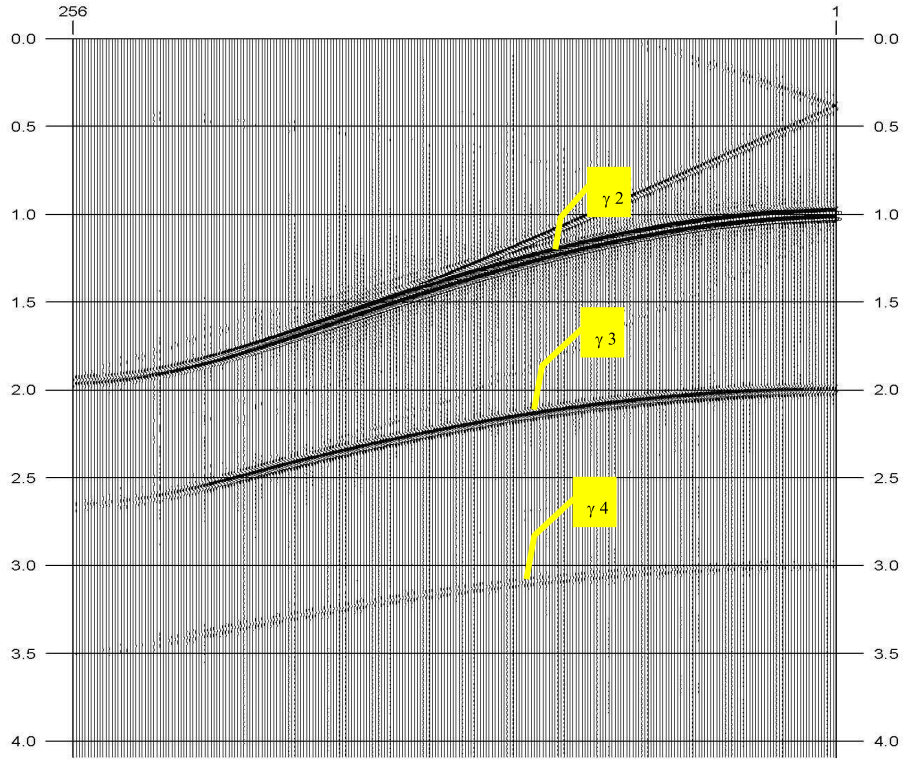

Figure 33. Virtual field constructed by multidimensional crosscorrelation of $P_a(x_r, x_s, \omega)$ with $V_b(x_r, x_s, \omega)$.

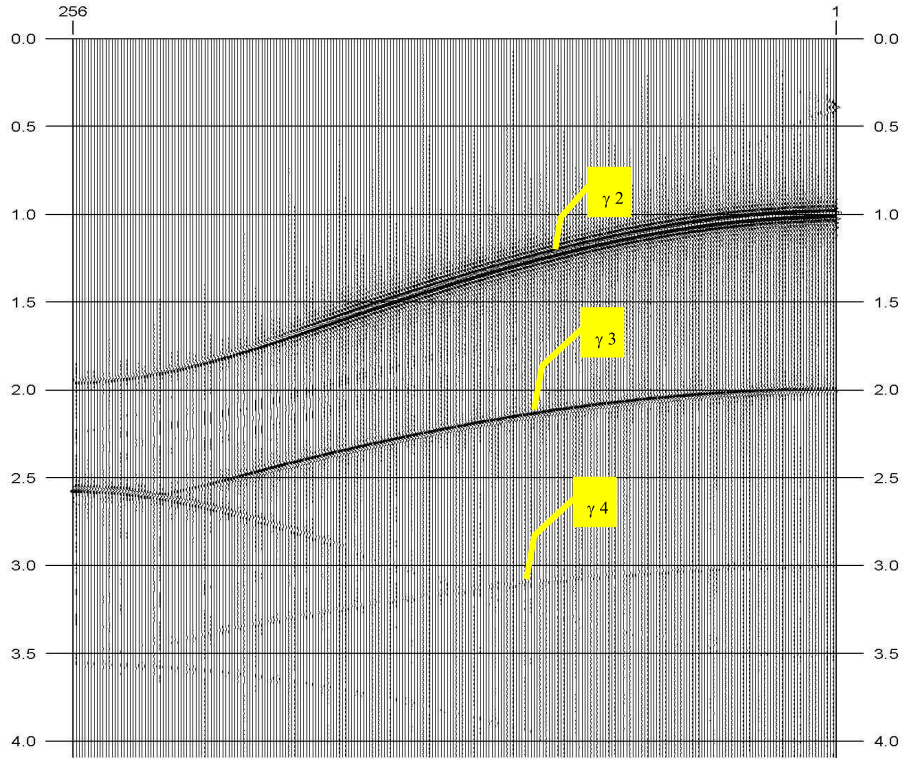

Figure 34. Renormalized virtual field constructed by multidimensional crosscorrelation of $P_a(x_r, x_s, \omega)$ with $V_b(x_r, x_s, \omega)$.

conjugate produces back propagation. With P_a in negative time, the virtual events remain causal.

As long as P_a contains only primary α_1, the virtual field contains only first-interface-related events, i.e., events that bring up information about the scattering points of the first interface. In the second iteration, the P_{2a} data set will include only the second primary, so that the virtual field will bring up information about the scattering points of the second interface only.

a. Renormalization

In the process of crosscorrelation, the amplitude of the events (real and virtual) changes, as well as the so-called correlation artifacts appear on the virtual field. To take care of the amplitudes and these artifacts, virtual events are renormalized in the construction of the virtual field. The renormalization can be achieved by replacing P_a^* in the computation of virtual events with P_a^{-1}. The field P_a^{-1} is defined as follows:

$$\int_{S_0} dS(x) P_a^{-1}(x_s, x, \omega) P_a(x, , x_r \omega) = \delta(x_s - x_r). \tag{3.9}$$

Thus equation (3.8) becomes

$$P_v'(x_r, x_s, \omega) = \int_{S_0} dS(x) P_a^{-1}(x, x_r, \omega) V_b(x, x_s, \omega), \tag{3.10}$$

where P_v' denotes the field of normalized virtual events.

Let us compare P_v and P_v' in the previous example by using P_a^{-1} instead of P_a^*. The renormalized virtual field P_v' is shown in Figure 34, and the correlation artifacts that we see on Figure 33 (P_v data) are gone.

C. Step 3: Prediction of internal multiples

After the construction of virtual events, the third step in the attenuation of internal multiples is a multidimensional convolution of virtual events with actual data, as in equation (3.6), this time using renormalized virtual events so that equation (3.6) is rewritten as follows:

$$P'_m(x_r, x_s, \omega) = \int_{S_0} dS(x) P'_v(x, x_r, \omega) V_b(x, x_s, \omega), \tag{3.11}$$

where P'_m denotes the field of renormalized internal multiples.

The field of virtual events for the construction of internal multiples is constructed by the crosscorrelation of the P_a data with the V_b data, and depicted in Figure 34 with seismogram and in Figure 35 with scattering diagrams. The field reveals only virtual reflections (primaries and multiples) that contain information about the first interface. All the constructed multiples in the first iteration are related to the first interface.

Note that convolution of the virtual data field with the particle velocity data field V_b constructs higher-order multiples more than once, just like the convolution between two data fields to construct free-surface multiples. But internal multiples are pretty weak to begin with, therefore the most significant ones will be the first-order internal multiples. Even though, the higher-order multiples can also be attenuated, as will be described later.

Let us examine the difference between the non-renormalized internal multiples in equation (3.6) [depicted in Figure 36], and the renormalized internal multiples in equation (3.11) [depicted in Figure 37]. The renormalized internal multiple amplitude looks more like the amplitude of the raw data than the non-renormalized internal multiple amplitude.

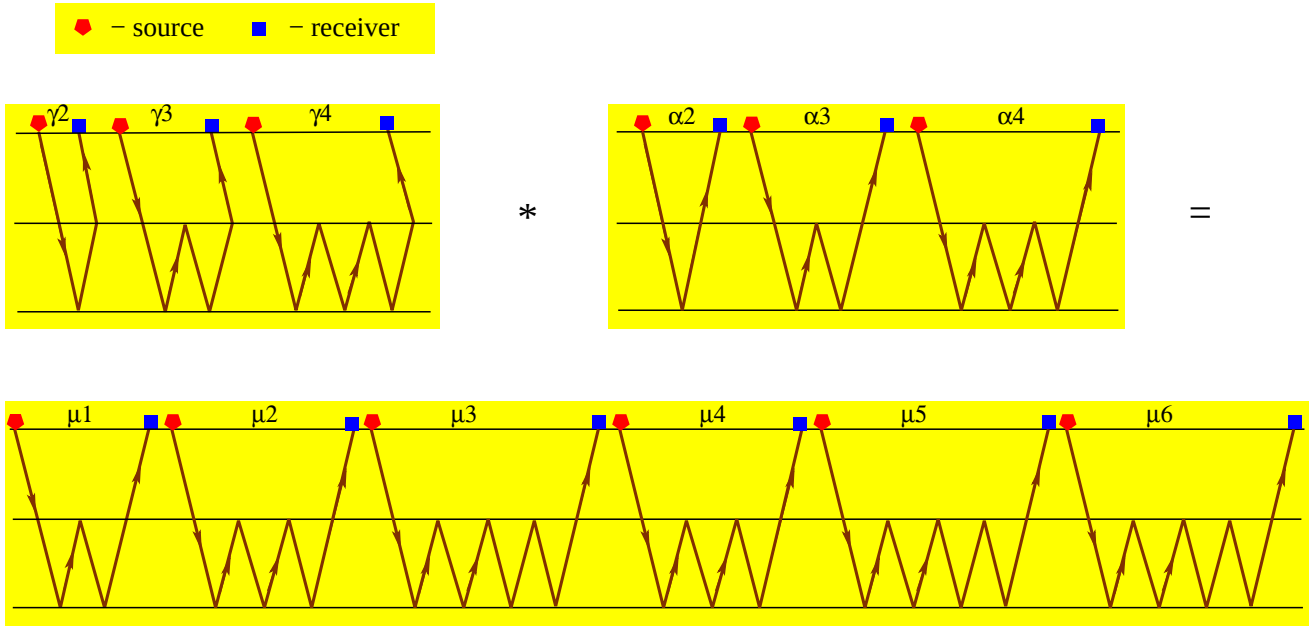

Figure 35. Scattering diagrams of construction of internal multiples.

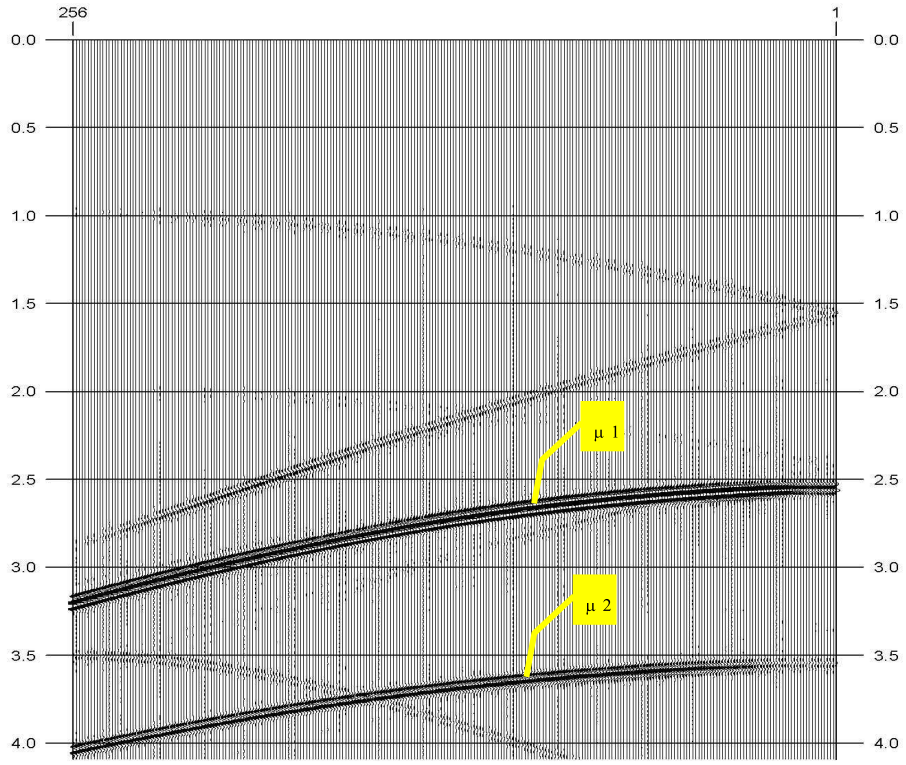

Figure 36. Non-renormalized internal multiples constructed by multidimensional convolution of the non-renormalized virtual events with $V_b(x_r, x_s, \omega)$.

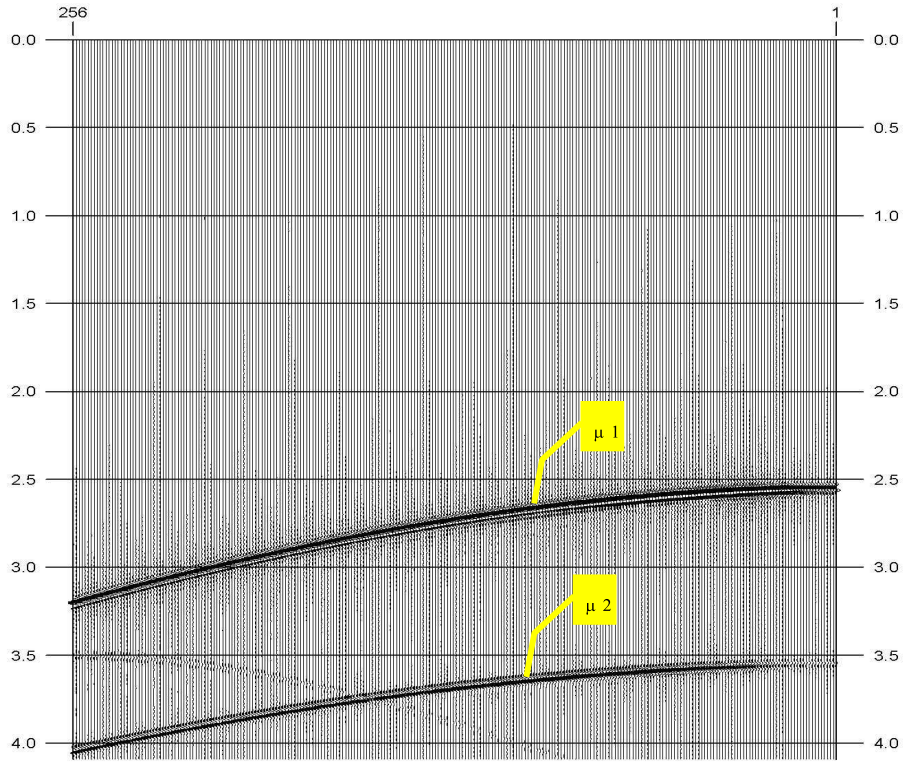

Figure 37. Renormalized internal multiples constructed by multidimensional convolution of the renormalized virtual events with $V_b(x_r, x_s, \omega)$.

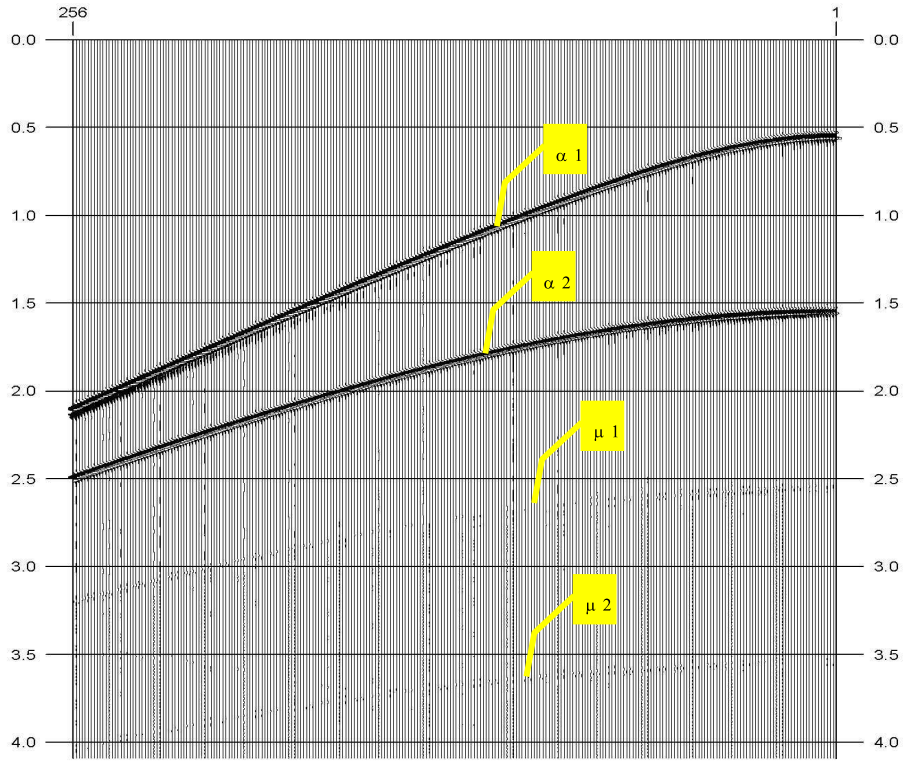

Figure 38. Demultipled data after removing first-order internal multiples.

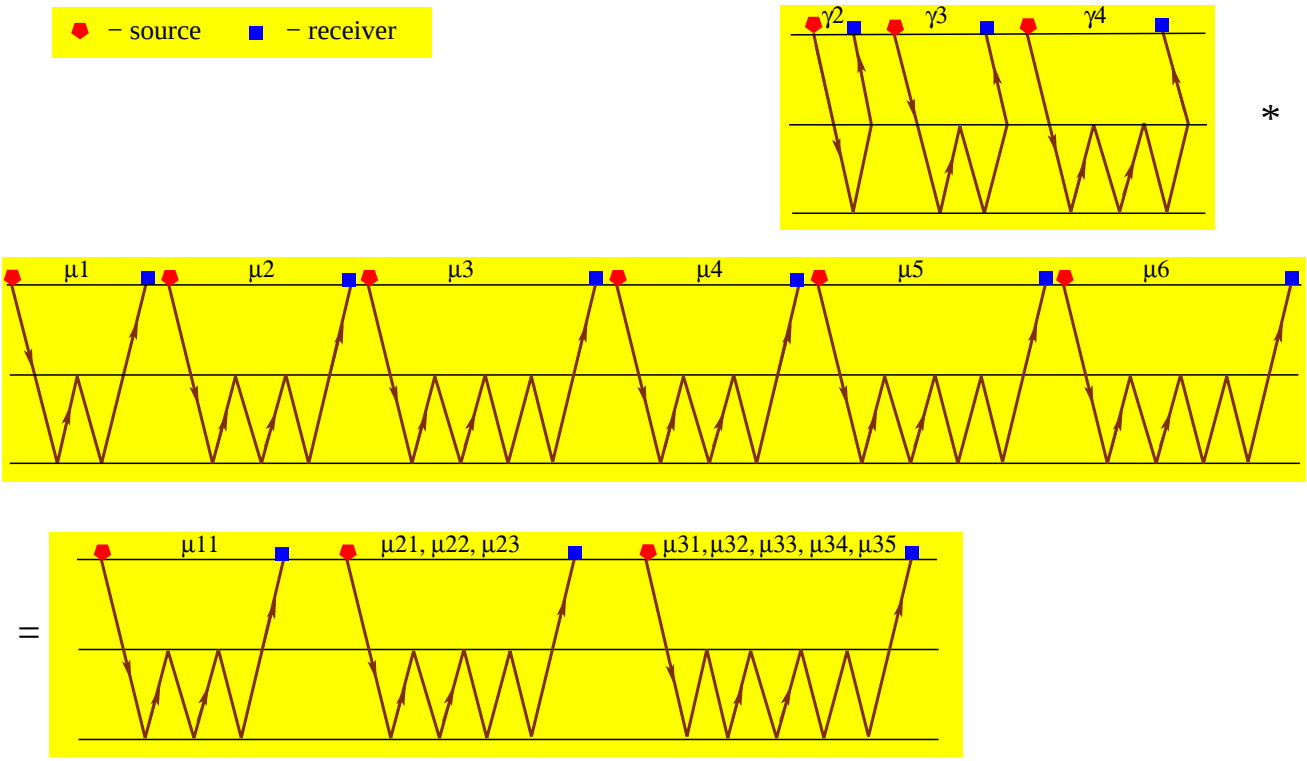

Figure 39. Second-order convolution of the virtual data field with the data field of the predicted internal multiples construct another field of internal multiples.

D. Step 4: Subtraction of internal multiples

The fourth step in the attenuation of internal multiples is a subtraction of the predicted multiples from the data. The demultipled data are shown in Figure 38. Compared to the original data, the internal multiples are much weaker.

E. Step 5: Demultiple of second-order internal multiples

As was mentioned earlier, the presented demultiple process constructs additional sets of higher-order[3] multiples. These are very weak, but can be attenuated even more. Just as in free-surface multiple construct, we can perform another convolution of the virtual data field with the data field of the predicted internal multiples (M_1), as explained by scattering diagrams in Figure 39, to construct another field of internal multiples M_2.

In the new construct, the primary virtual event γ_2 combines with the first-order predicted internal multiple μ_1, and constructs second-order internal multiple μ_{11}. The virtual event γ_3 combines with the first-order predicted internal multiple μ_1 to construct third-order internal multiple μ_{21}, as well as combination of the primary virtual event γ_2 with the second-order predicted internal multiples μ_2 and μ_4, construct two third-order internal multiples μ_{22} and μ_{23}, so we have three third-order internal multiples. By combining γ_2 with μ_3, μ_5 and μ_6, as well as by combining γ_3 with μ_2 and μ_4, and by combination of γ_4 with μ_1, we construct fourth-order internal multiples.

Subtraction of the second multiple field from the first multiple field will leave us with only one set of first- and second-order multiples, which we can now remove from

[3]Similarly to free-surface multiples, the order of internal multiple corresponds to the number of bounces at the subsurface interfaces. In other words, the first-order internal multiple bounces one time at any interface (Figure 35, μ_1), the second-order internal multiple bounces twice at any interface (μ_2 and μ_4), and the third-order internal multiple bounces three time at any interface (μ_3, μ_5, and μ_6).

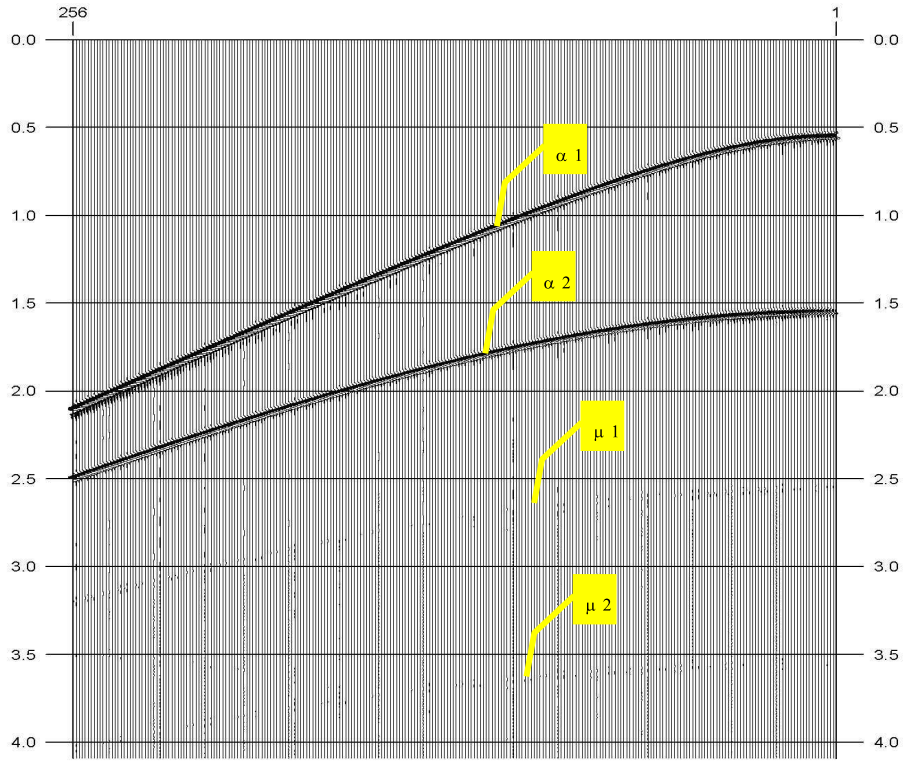

Figure 40. Demultipled data after removing second-order internal multiples.

the data:

$$DM = D - (M_1 - M_2), \tag{3.12}$$

where DM is the demultiple data and D is the original data. Of course, now we have constructed a few additional third- and higher-order internal multiples, that are even weaker than second-order internal multiples.

Actually, we can go even further and perform another convolution with M_2, and then another convolution with M_3, and so on, producing new series for each BIMG location:

$$DM = D - (M_1 - M_2 - M_3 - M_4 - \ldots) \tag{3.13}$$

In our example, the prediction and subtraction of these second-order internal multiples clears the data from the multiples pretty good, as shown in Figure 40, there is no visible residue of the internal multiples. Higher-order internal demultiple is not required.

F. Step 6: Another iteration with a different division

The next step is to perform a division at a new BIMG location. Note that we do not divide the original data again; we divide the second part of the data, P_b and V_b, because we have already taken care of the first-interface related events (virtual and multiples), and do not want the first primary in our calculations again. It is also correct if the first part of the first BIMG division (P_a and V_a) contains more than one primary. As soon as the primaries in P_a took their part in construction of corresponding virtual events, we are done with them and do not need them for the second iteration.

In the previous example the model contains only two reflectors, i.e. the internal multiples have scattering points only at the first interface, and since we have

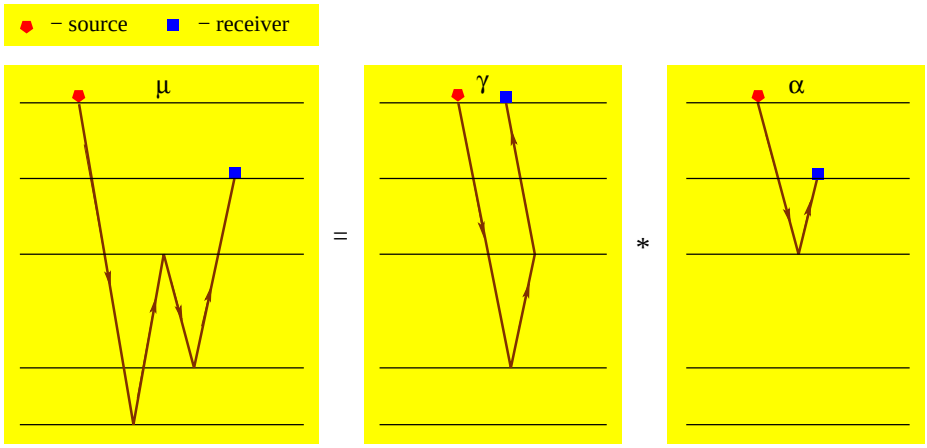

Figure 41. Construction of an internal multiple in OBS data using virtual events from towed-streamer data.

already removed the first-interface related multiples, there is no second iteration. We need at least four layers (three reflectors) to make two iterations in internal-multiple attenuation. The data are demultipled and ready for imaging.

4. Expanding the technique of internal multiple attenuation to OBS data

In towed-streamer acquisition, both source and receiver are located near the free surface, which allows us to introduce the convention of wavelet extrapolation to the free surface. In OBS acquisition the source is on the free surface, but the receivers are attached to the ocean bottom.

To make the technique of attenuation of internal multiples work, we must combine OBS data with towed-streamer data in the same location, just like it has been done in free-surface multiple attenuation (Ikelle, 1999). The technique uses virtual field constructed from towed-streamer data, and velocity field from OBS data, as described in Figure 41. Multidimensional convolution of the virtual event γ with the primary α constructs the internal multiple μ that belongs to OBS data.

5. Conclusions

We have shown that virtual events can be used to construct multiples in a way similar to the construction of free-surface multiples. The procedure requires six steps:

1. applying the BIMG concept,
2. constructing the virtual field,
3. predicting internal multiples,
4. subtracting constructed internal multiples,
5. Demultiple of second-order internal multiples, and
6. another round with a different BIMG.

Renormalization is required for predicting proper amplitudes of internal multiples.

Demultiple of first-order multiples attenuates the most problematic internal multiples. Another multidimensional convolution of the virtual field with the predicted multiple field, allows us to remove second-order multiples as well.

CHAPTER IV

A NUMERICAL EXAMPLE OF INTERNAL MULTIPLE ATTENUATION

Imaging of sub-basalt layers in areas like the Voring and More basins off mid-Norway, basins in the Faroes, West Greenland, Angola, and Namibia basins; the Brazil margins, the Western Australian basins; and the Deccan Traps of India is very important today, as these basaltic basins are known to be potential hydrocarbon reservoirs. The basalts that have intruded the sedimentary rocks are known to have increased maturation of sub-basalt source rocks due to increased burial.(Singh, 2005).

In this chapter, I will run the internal multiple attenuation process on 1D acoustic model, which contains basalt layer and sub-basalt sediments. Basalt layers have high impedance, therefore should produce relatively strong internal multiples. Since sub-basalt primaries have weaker amplitudes than other primaries, strong internal multiples will interfere with data interpretation.

Generally, the first iteration of the demultiple is the main one, because it is removing the strongest internal multiples. Ikelle et al. (2003) indicate that free-surface multiples with first and last bounces below the first BMG reflector are quite weak, especially in deeper-water cases. Since internal multiples are weaker than free-surface multiples and we are attenuating mainly first-order internal multiples, internal multiples that bounce below the BIMG reflector should not constitute a problem. Therefore, I will apply the BIMG concept only one time.

In the first section I will describe the model I use to demonstrate the internal-multiple-attenuation technique, and I will explain the difficulties presented by this model. In the second section, I will show the generated data. In the third section, I will go through the demultiple process and present the predicted internal multiples. In the fourth section, I will discuss the demultipled data.

1. About the model

According to Singh (2005), imaging of sub-basalt layers is very difficult. Very little energy passes through the basalt layer because the basalt has high velocity and density compared to the surrounding sedimentary layers. Most energy reflects back from the basalt-sediment interface due to high-impedance contrast between the basalt layer and the sediments. Multiples reflected from the basalt-sediment interface interfere with the primary reflections, in some cases leading to misinterpretation of various events.

The strongest multiples are the free-surface multiples which have reflected from the top of the basalt layer. Attenuation of these free-surface multiples is described in details by Singh (2005).

Another high-impedance contrast is the interface between the water layer and the first layer of the sea basin. Internal multiples, which have most of their energy reflected from the top of the basalt layer, bounce on the sea floor and still keep most of the remaining energy due to the high-impedance contrast between the water and the first layer of the sea basin. They reflect again from the basalt layer, and then they are recorded by geophones.

I will use the internal-multiple attenuation technique described in the previous chapter to attenuate internal multiples in the 1D basalt-sediment model. The model is presented in Figure 42. It has a water layer on the top, fife sediment layers, a basalt layer, and three layers of sub-basalt sediments.

2. About the data

Figure 43 depicts the pressure data simulated by the above model. The data contains of nine primary reflections and many internal multiples. The first primary, α_1, is

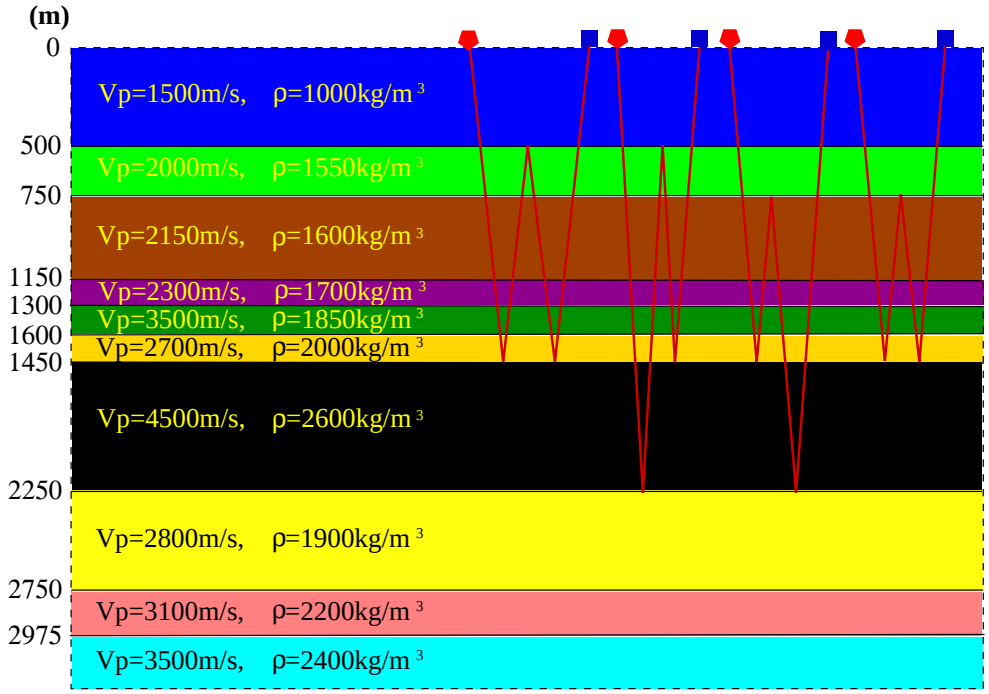

Figure 42. 1D acoustic model, that represents basalt and sedimentary layers under water layer.

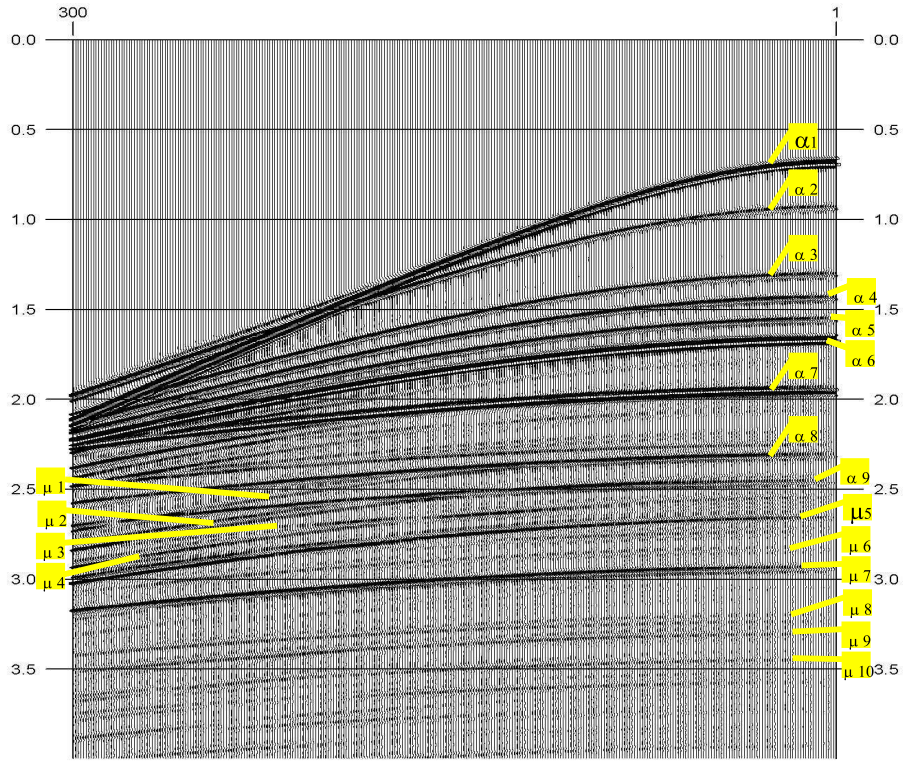

Figure 43. Pressure data simulated by the basalt-sediment model.

reflected from the sea floor. The sixth and seventh primaries, α_6 and α_7, are reflected from the top and bottom of the basalt layer, respectively. α_1, α_6, and α_7 have high amplitude compared to other primaries, a difference which can be detected visually.

Primaries α_2, α_3, α_4 and α_5 are reflections from the sediment layers above the basalt layer. Primaries α_8 and α_9 are reflections from the sub-basalt layers. Primaries α_8 and α_9 are visibly weaker comparing to α_2, α_3, α_4, and α_5. The dispersion of the energy is not enough to explain this difference in the amplitudes; the difference is due to the basaltic layer in the model, as was explained in the previous section.

The most significant internal multiples, as I pointed out in the previous section, are the multiples reflected from the basalt layer and bounced on the sea floor, such as μ_5 and μ_7[1]. They correspond to the multiples shown on the model in Figure 42.

Some internal multiples, such as μ_1 and μ_2, are 'hiding' behind primaries in the near offsets, but 'come out' at the far offset.

Note also that sub-basalt primaries α_8 and α_9 are interfered, especially primary α_9.

3. Prediction of internal multiples

Let me apply the technique for the attenuation of internal multiples, described in the previous chapter. First, I put my BIMG reflector just below the second reflector, so I mute the data under the second primary to receive the first part – pressure data P_a, depicted in Figure 44. The second part – particle velocity data V_b is depicted in Figure 45. The predicted multiples are shown in Figure 46. Let us take a close look at this figure.

The events in this figure have two slopes at the far offset. That reflects the fact

[1]The numbers given to the multiples do not reflect their arrival order, but are used to point out some multiples that will be attenuated.

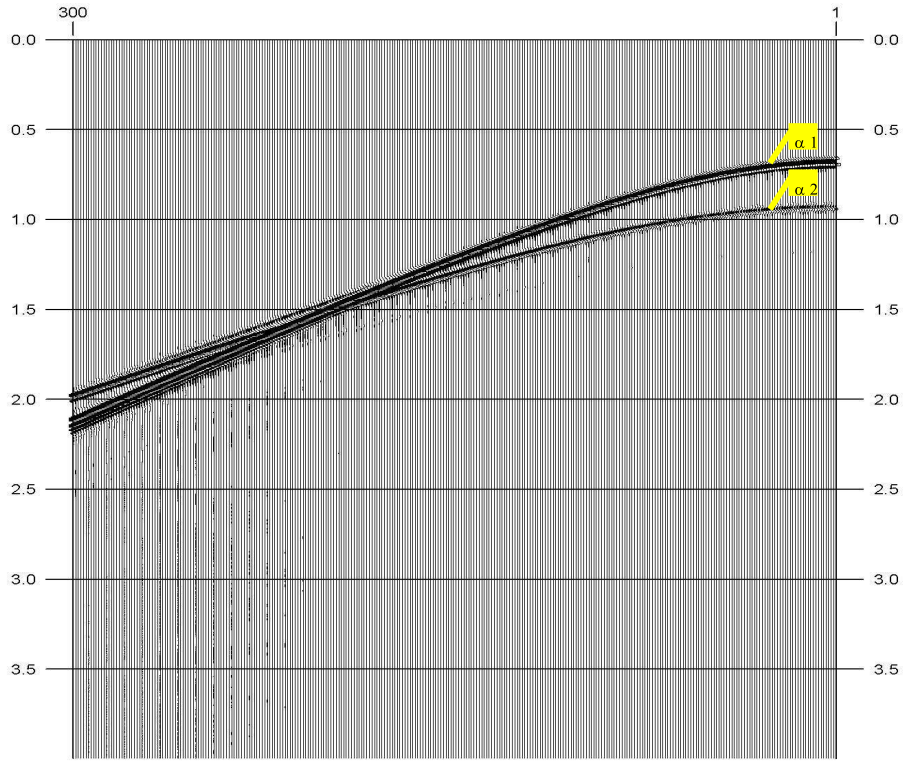

Figure 44. Pressure data P_a.

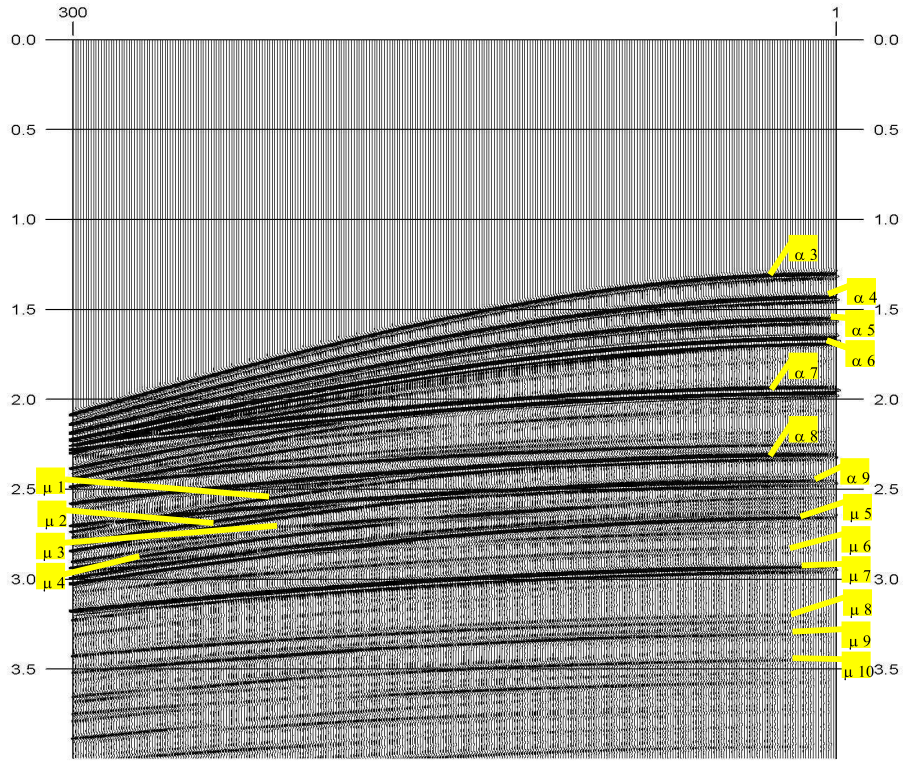

Figure 45. Particle velocity data V_b.

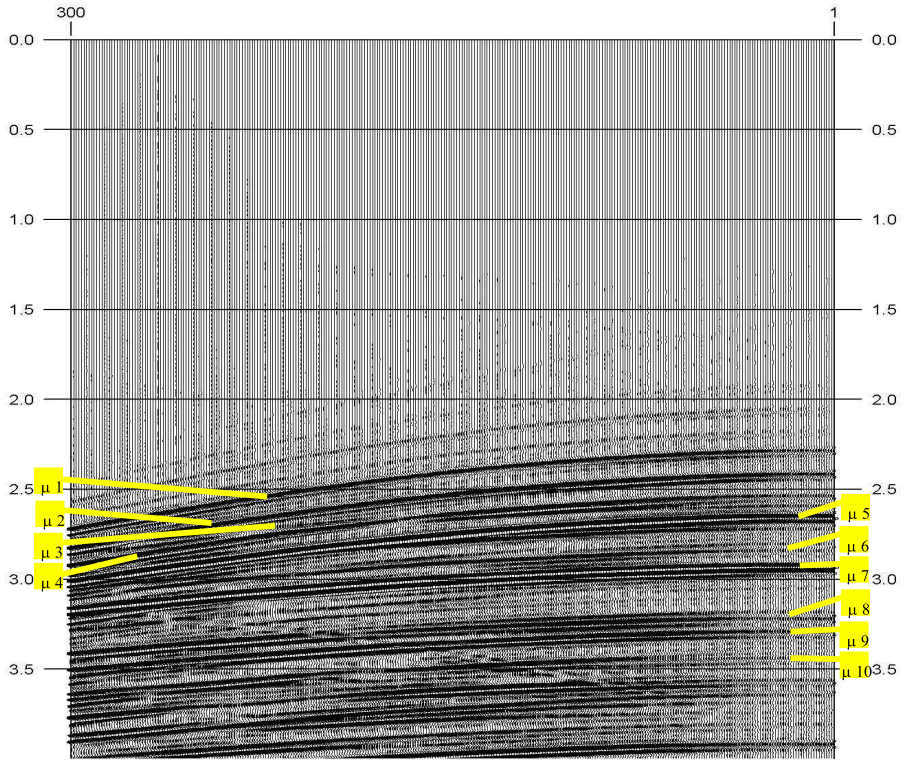

Figure 46. Predicted internal multiples.

that the data set P_a consists of two primaries, which means that the constructed multiples bounce at the first and/or second interfaces.

Also, multiples μ_5 and μ_7 are more noticeable than others. Event μ_7 seems to have more energy than event μ_5, but predicted-multiple field reveals that two events have been combined in μ_7 (look at the different slopes at the far offset): one of these two internal multiples has bounced on the first interface. The other one has bounced on the second interface.

4. Demultipled data

Subtraction of the predicted multiples from the original data shows significant improvement, as shown on the demultipled data in Figure 47. Internal multiple μ_7 has been attenuated, leaving a very small residue. Internal multiple μ_7 has been almost entirely attenuated leaving residue at the far offset.

Multiples μ_1 and μ_2 have been attenuated, so that primaries α_8 and α_9 are now not interfered by these multiples, their amplitudes are clearer, and they can be followed easily through all the offsets. Multiples μ_3, μ_4, μ_6, μ_8, μ_9, and μ_{10} are attenuated as well.

The internal multiples that interfere with basalt reflections were not attenuated in this iteration.

5. Conclusions

In this chapter I have tested the technique for attenuation of internal multiples presented in the previous chapter. I chose a model that includes a basalt layer to receive strong internal-multiple reflections.

The demultipled data show significant improvement compared to the raw data.

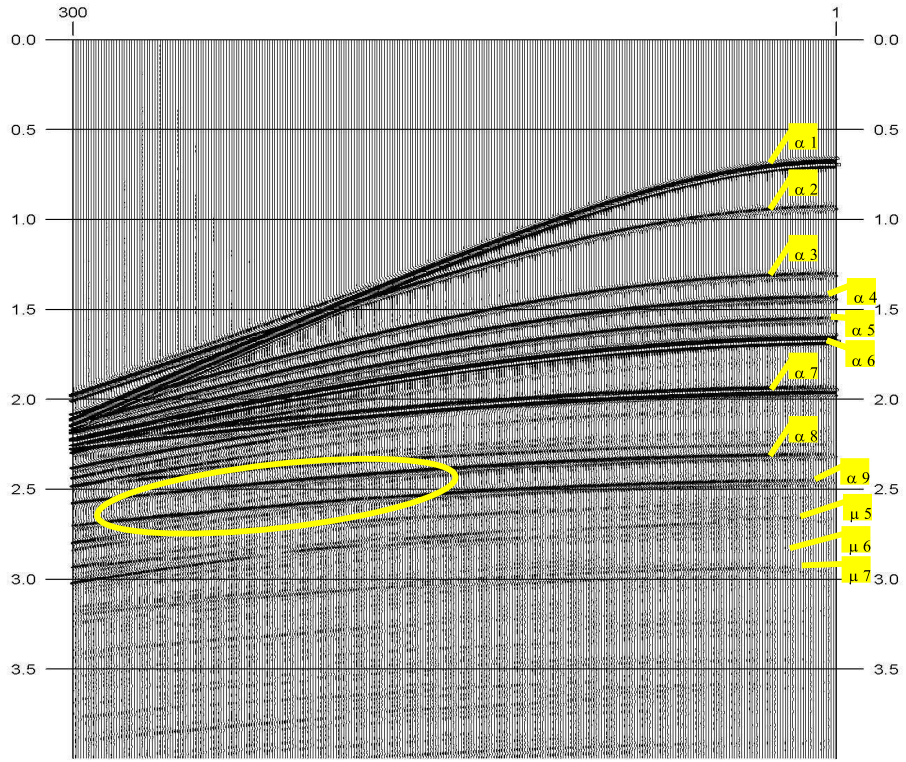

Figure 47. Demultipled data.

The first iteration attenuates most problematic internal multiples: μ_5 and μ_7 (because of the strong energy), and μ_1 and μ_2 (because they interfere with weak sub-basalt primaries).

The multiples that interfere with basalt primaries were not attenuated. To attenuate these internal multiples we have to run another iteration. Luckily, basalt primaries have strong energy, and the interfering internal multiples are relatively weak in comparison.

CHAPTER V

CONCLUSIONS

I have shown numerically that the attenuation of internal multiples can be achieved from surface data only by using the concept of virtual events. This multiple-attenuation technique does not require a priori knowledge of the subsurface model, though basic interpreter judgment is needed [i.e., identifying the first primaries for the first part of the data, $P_a(x_r, x_s, \omega)$].

The 1D model used in the numerical simulation included high-impedance contrast at the interfaces of water-sediment and sediment-basalt. Thus the data generated by the finite-difference modeling technique contain a significant amount of internal multiple energy. I show the effectiveness of my methods even for this complex case. Moreover, the demultiple results clearly show primaries which are quite obscure in the raw data due to interferences between internal multiples and primaries.

Another important contribution of this thesis is that I present a thorough review of the concept of virtual events. I show that virtual events are created by crosscorrelation between two data fields, $P(x_r, x_s, \omega)$ and $V(x_r, x_s, \omega)$, and that they involve forward and backward wave propagation. Further, I show that virtual events obey physical laws. I arrived at this conclusion by confirming the findings of Ikelle and Gangi (2006) that virtual events are included in the representation theorem along with actual events. I also point out that virtual events are not recorded by current acquisition technology but can be constructed from the actual data.

I also put the concept of virtual events in a larger context by discussing their analogy to left-handed materials (i.e., materials with a negative refraction index) discovered in the last three years in optics. I basically show that virtual events obey Snell's law just like light in left-handed materials.

I have proposed a physical interpretation of virtual events: namely, that virtual events represent the time spent in a number of contiguous subsurface layers (including the special case of a single layer).

The attenuation of internal multiples is not the only application of the concept of virtual events. I believe that virtual events will be used in additional geophysical applications in the near future.

REFERENCES

Berkhout, A. J., and Verschuur, D. J., 1997, Estimation of multiple scattering by iterative inversion, part i: theoretical considerations: Geophysics, **62**, 1586–1595.

de Hoop, A., 1966, An elastodynamic reciprocity theorem for linear viscoelactic media: Appl. Sci. Res., **16**, 39–45.

de Hoop, A. T., 1995, Handbook of radiation and scattering of waves: Academic Press, San Diego, CA.

Gangi, A. F., 1970, A derivation of the seismic representation theorem using seismic reciprocity: J. Geophys. Res., **75**, 2088–2095.

Hansen, R. F., 1948, Multiple reflections of seismic energy: Geophysics, **13**, 58–85.

Houck, A. A., Brock, J. B., and Chuang, I. L., 2003, Experimental observations of a left-handed material that obeys snell's law: Physical Review Letters, **90**, 137401.

Ikelle, L. T., and Amundsen, L., 1997, Multiple attenuation at primary/multiple interferencess: the troll example: The Leading Edge, **16**, 1751–1753.

Ikelle, L. T., and Amundsen, L., 2002, Noniterative multiple attenuation methods: linear inverse solutions to nonlinear inverse problems: The Leading Edge, **21**, 350–356.

Ikelle, L. T., and Gangi, A. F., 2005, New type of reflections in inhomogeneous media is revealeed by an analysis of scattering diagrams of the correlation-type representation theorem: J. Seismic Explor., **14**, 1–12.

Ikelle, L. T., Amundsen, L., Gangi, A. F., and Wyatt, S., 2003, Kirchhoff scattering series: insight into the multiple attenuation method: Geophysics, **68**, 16–28.

Ikelle, L. T., Osen, A., Amundsen, L., and Shen, Y., 2004, Noniterative multiple attenuation methods: linear inverse solutions to nonlinear inverse problems -ii. bmg approximation: Geophysical Journal International, **159**, 923–930.

Ikelle, L. T., 1999, Combining two seismic experiments to attenuate free-surface multiples in obs data: Geophysical Prospecting, **47**, 179–194.

Ikelle, L. T., 2006, A construct of internal multiples from surface data only: the concept of virtual events: Geophysical Journal International, **164**, 383–393.

Jakubowicz, H., 1998, Wave equation prediction and subtraction of rnterbed multiples: Expanded Abstr., 68th Ann. Internat. SEG Mtg., New Orleans, pages 1527–1530.

Robinson, E. A., 1957, Predictive decomposition of seismic traces: Geophysics, **22**, 7676–778.

Schneider, W. A., Prince, E. R., and Giles, B. F., 1965, A new data-processing technique for multiple attenuation exploiting differential normal moveout: Geophysics, **30**, 348–362.

Singh, S. K., December 2005, Sub-basalt imaging: modeling and demultiple: Master's thesis, Texas A&M University, College Station, TX.

Sommerfeld, A., 1954, Optics: Academic Press, New York.

Watts, A. O., and Ikelle, L. T., 2006, Linear demultiple solution based on the concept of bottom multiple generator (bmg) approximation: Geophysical Prospecting, in press.

Weglein, A. B., Gasparotto, F. A., Carvalho, M., and Stolt, R. H., 1997, An inverse scattering series for attenuating multiples in seismic reflection data: Geophysics, **62**, 1975–1989.

VITA

Name:	Ilana Erez
Address:	H.M. Shapira 4/15 Ashdod, Israel
E-mail address:	lanaerez@yahoo.com
Education:	B.Sc. (Geophysics), Tel Aviv University, Tel Aviv, Israel (2003) M.S. (Geophysics), Texas A&M University, College Station, TX (2006)